Physics – Uspekhi **57** (3) 234 – 249 (2014)

100th ANNIVERSARY OF THE BIRTH OF Ya B ZELDOVICH

PACS numbers: 52.80.Mg, 82.33.Vx, 88.20.jj

From combustion and detonation to nitrogen oxides

M F Ivanov, A D Kiverin, B A Klumov, V E Fortov

DOI: 10.3367/UFNe.0184.201403c.0247

Contents

1. Introduction **234**
2. Transient combustion of gaseous mixtures **234**
2.1 Initiation of combustion and settling of different combustion modes; 2.2 Initiation of combustion waves by localized thermal energy sources; 2.3 Inflammation near concentration limits
3. Flame acceleration and transition to detonation in channels **241**
4. Production of nitrogen oxides in heated air **244**
5. Conclusions **248**
References **249**

Abstract. This paper looks at Ya B Zeldovich's ideas on the combustion and detonation physics of gaseous mixtures and how they evolved as work in this field progressed. The paper demonstrates the fundamental role of Zeldovich's concept of spontaneous combustion waves in studying transient initiation processes for various combustion regimes and in determining the energy and concentration inflammation limits for combustible gaseous mixtures. It shows how his notion that flame front stretching crucially influences flame acceleration in channels explains in a new way the deflagration-to-detonation transition in highly reactive gaseous mixtures. Most of the presented results were obtained by simulations, allowing Zeldovich's ideas to be extended to the combustion of real gaseous mixtures, where chemical reactions and gasdynamical flows add hugely to the complexity of the problem. The paper concludes by using Zeldovich's mechanism to assess the amount of nitrogen oxide produced by a lightning discharge.

1. Introduction

In the wealth of Yakov Borisovich Zeldovich's scientific studies, which have become classical in quite different areas of physics — from gas dynamics to cosmology — a series of studies concerned with combustion and detonation stands out. Throughout his impressive and surprisingly productive creative life, Yakov Borisovich took a vivid interest in the progress of combustion and detonation science, calling it an "evergreen" subject. By addressing this subject area for nearly 40 years, Ya B Zeldovich created, in fact, the foundation of the modern science of combustion of gaseous and condensed media. The results obtained in his work, beginning with the earliest, immediately become classical and not require revision. Ya B Zeldovich produced an extremely clear description of the complex nonlinear interrelations determining the exothermal processes both in the subsonic deflagration and supersonic detonative combustion modes. This made it possible to provide qualitative answers to the fundamental questions which arose in applied problems over many years. A quantitative and more detailed analysis of the problem became possible with the advent of high-performance computers.

In this review, we endeavor to track what role the findings and concepts formulated by Ya B Zeldovich play in the solution of several problems of combustion and detonation of combustible gaseous mixtures at the modern stage of research.

M F Ivanov, A D Kiverin, B A Klumov, V E Fortov Joint Institute for High Temperatures, Russian Academy of Sciences,
ul. Izhorskaya 13/2, 125412 Moscow, Russian Federation
E-mail: ivanov_mf@mail.ru, alexeykiverin@gmail.com,
klumov@mpe.mpg.de, fortov@ras.ru

Received 13 December 2013, revised 14 January 2014
Uspekhi Fizicheskikh Nauk **184** (3) 247 – 264 (2014)
DOI: 10.3367/UFNr.0184.201403c.0247
Translated by E N Ragozin; edited by M S Aksent'eva

2. Transient combustion of gaseous mixtures

Active investigations into the processes of combustion of gaseous mixtures, which go back to more than a century ago, are due to the decisive role played by these processes in the problems of improving the efficiency of a broad class of power devices and the problems of lowering the risks and scale of damage in severe industrial accidents. To date, settled theoretical notions have formed about the processes determining the stationary modes of combustion and detonation. However, in real situations of limited space [be it the combustion chamber of an engine, a gaseous-fuel storage, a coal mine, or the reactor hall of an nuclear power plant (NPP)] the propagation of combustion waves is a sequence of nonstationary, including transient, modes caused by a variety of nonlinearly interacting physicochemical factors. Below, we consider the development of combustion of gaseous mixtures throughout the process — from ignition to the transition from slow combustion to detonation. Our analysis will rely primarily on the data of mathematical simulations of the combustion of hydrogen-oxygen and hydrogen-air mixtures.

Ya B Zeldovich's work on the theory of propagation of stationary combustion [1–5] and detonation [6] waves is basic to the modern theory of stationary combustion modes. The

problems solved by Ya B Zeldovich on the propagation conditions of an exothermal reaction wave in a mixture and on combustion modes in a nonuniformly heated gas [7] are of significance in explaining the physics of transient ignition, combustion, and detonation.

2.1 Initiation of combustion and settling of different combustion modes

Leaning upon the results of Ref. [8] by A N Kolmogorov, I G Petrovskii, and N S Piskunov about the limiting solutions of diffusion equations with a source term, Ya B Zeldovich introduced the notion of combustion wave propagation velocity as an intermediate asymptotics, correct with limited accuracy in a restricted spatial domain during a limited time interval. This approach allowed him to formulate the concept of a spontaneous combustion wave [7], which consists in the following: in media with a nonuniform distribution of reaction rate, the reaction which generates the combustion wave begins nonsimultaneously and independently at every spatial point. The onset of exothermal reaction corresponds to the point with the shortest induction time $\tau_{\rm ind}$ (the time of the onset of the intense exothermal reaction caused by the recombination of the radicals accumulated during the induction stage). Therefore, inflammation at each spatial point takes place with some delay relative to the neighboring point at which the reaction rate is higher. When the medium is characterized by a negative gradient of the reaction rate (for instance, due to a temperature decrease or a combustible component concentration decrease from the stoichiometric value), the propagation velocity of the spontaneous reaction wave is expressed as

$$U_{\rm sp} = \left| \frac{{\rm d}\tau_{\rm ind}}{{\rm d}x} \right|^{-1} . \qquad (1)$$

For a given chemically active mixture, the spontaneous reaction wave velocity is independent of the thermal conductivity, diffusion, or sonic speed and is determined only by the value of initial temperature nonuniformity. When considering spontaneous wave motion over the temperature gradient, it is possible to obtain the energy inflammation criteria, the concentration criteria are derived in a similar way by specifying the concentration gradient. For a nonzero temperature gradient [7], the spontaneous wave velocity is defined exclusively by its magnitude and the characteristics of reaction behavior in relation to the temperature $({\rm d}\tau_{\rm ind}/{\rm d}x = (\partial\tau_{\rm ind}/\partial T)\,\partial T/\partial x)$.

Two extreme cases are naturally singled out: with $\partial T/\partial x = 0$ and $\partial T/\partial x \to \infty$. The zero temperature gradient corresponds to the case of volume (volumetric) explosion, whereby the reaction is initiated simultaneously at all the spatial points; a small departure of the gradient from zero generates an essentially supersonic exothermal reaction wave, which produces a pressure wave behind its front. The resulting wave structure asymptotically forms into a detonation wave [9]. The infinite gradient corresponds to the combustion wave initiation by a point source in a mixture which does not react at the initial temperature. No spontaneous wave emerges in this case; a wave of normal combustion is formed instead, which propagates due to thermal conductivity and diffusion, and the problem boils down to that of thermal flame propagation [1–5].

Therefore, the velocities of combustion waves initiated by spatial temperature nonuniformity are bounded below by the velocity of normal combustion and above, respectively, by the Chapman–Jouguet detonation velocity. The question about the initiation of other possible combustion modes — from slow to detonative combustion, depending on the initial nonuniform conditions in a combustible mixture — was first posed in Ref. [7].

For a single-step exothermal reaction model, Ya B Zeldovich proposed the following combustion mode classification in relation to the initial conditions, which define the relationships between the spontaneous combustion wave velocity $U_{\rm sp}$ and the characteristic velocities of the problem: the normal laminar flame velocity $U_{\rm f}$, the sonic speed $a_{\rm f}$ in an unperturbed medium, and the Chapman–Jouguet detonation velocity $U_{\rm CJ}$.

I. For $U_{\rm sp} > U_{\rm CJ}$, i.e., as the zero temperature gradient limit is approached, a so-called weak detonation wave forms, in which the pressure behind the wave front is lower than $p_{\rm CJ}$ but higher than the pressure for an adiabatic explosion.

II. For $a_{\rm f} \leqslant U_{\rm sp} \leqslant U_{\rm CJ}$, the exothermal reaction wave travels with a supersonic velocity, which determines the proximity of the characteristic chemical and gas-dynamic time scales ($t_{\rm chem} = L/U_{\rm sp}$ and $t_{\rm gas} \sim L/a_{\rm f}$). The pressure wave generated due to energy release in the reaction zone may be enhanced simultaneously with the energy release and may form a Chapman–Jouguet detonation wave after a transient period. This mode, which was first demonstrated numerically in Ref. [9], has repeatedly attracted the attention of researchers in the area of direct detonation initiation.

III. For $U_{\rm f} < U_{\rm sp} \ll a_{\rm f}$, the reaction wave propagates at a subsonic velocity, the sound waves manage to equalize the pressure over the characteristic chemical scale lengths, and the influence of gas-dynamic effects turns out to be insignificant. The pressure in the reaction zone remains nearly constant; however, since the reaction velocity has a finite nonzero value, the mode of 'fast combustion' is realized ahead of the wave front, with a velocity $U_{\rm sp} > U_{\rm f}$, which are intermediate asymptotics, according to Ref. [7].

IV. For $U_{\rm sp} < U_{\rm f} \ll a_{\rm f}$, as discussed above, a spontaneous wave does not emerge, the reaction wave propagation is determined exclusively by thermal conductivity and diffusion, and a combustion wave with a normal velocity $U_{\rm f}$ is initiated.

After the publication of Ya B Zeldovich's papers [7, 9], the problem of combustion and detonation wave initiation was repeatedly solved analytically and numerically with the use of the conception of spontaneous combustion wave (see, for instance, Refs [10–12]). In the majority of studies, the problem was posed to determine the detonation formation conditions for the purpose of using them to interpret the mechanisms of direct detonation initiation, the transition from slow combustion to detonation, or the emergence of 'knock' in the chambers of internal combustion engines (ICEs). In the calculations, as a rule, one used of single-step exothermal reaction models; in this case, the difference between the calculated ignition energy values and the experimentally measured ones ranged up to two orders of magnitude. Large errors should be expected with the use of single-step exothermal reaction models, because such simplified models do not reflect many basic features of real reaction mechanisms. In Ref. [13], an investigation was made of detonation initiation in mixtures in which combustion was described by a two-stage reaction; this permitted a qualitative substantiation of the necessity to include the ignition

mechanism so as to reproduce the characteristics of detonation formation in combustible mixtures.

Next we enlarge on the description of the formation mechanisms of different combustion modes of hydrogen and hydrocarbon combustible mixtures, whose detailed chemical ignition kinetics cannot be correctly described by a single-step Arrhenius reaction. References [14, 15] are devoted to the solution to the problem of spontaneous combustion in the presence of a temperature gradient with the inclusion of the detailed mechanism of reaction progress by the example of hydrogen-air and hydrogen-oxygen mixtures.

In this section, our exposition hereafter is based on the results of Ref. [15]. We consider the ignition of a hydrogen-oxygen mixture, for which the chemical kinetics is relatively simple, the most reliable, and adequately studied. Unlike the chemical kinetics of hydrocarbon fuels, which comprises up to several thousand reactions for several hundred intermediate components, the hydrogen kinetics are usually described by two tens of reactions for eight basic reagents: H_2, O_2, H_2O, H, O, OH, HO_2, and H_2O_2 (see, for instance, Refs [16–19]).

Under normal conditions, hydrogen reacts with oxygen in two global stages: (1) the decay of mixture reagents with the formation and accumulation of radicals, which proceeds with hardly any energy release, and (2) exothermal reactions of radical recombination and chain termination. At a given temperature and pressure, the exothermal reaction begins after a lapse of time — the induction time $\tau_{\rm ind}$ — which varies along the temperature gradient and defines the formation of a spontaneous combustion wave. The temperature dependence of the induction time for a fixed mixture composition and pressure has a feature defined by the temperature T_1, at which the induction time is on the order of the exothermal reaction time. This characteristic is sometimes referred to as the 'extended second ignition limit'. For a stoichiometric mixture of hydrogen with oxygen or air, T_1 is on the order of 1100–1200 K. For $T > T_1$, the induction times are short and their temperature dependence is rather flat, and so in the region of the temperature gradient with $T > T_1$ one would expect rather high velocities of spontaneous combustion waves (the magnitude of $\partial\tau_{\rm ind}/\partial T$ is small), which become lower with propagation along the temperature gradient towards the region of lower temperatures and, as a consequence, longer induction times. In moving to the low-temperature region ($T < T_1$), the spontaneous wave velocity will exhibit a stepwise decrease. Therefore, one would expect a qualitative difference in the process dynamics when the maximum temperature in the gradient is assigned for $T^* < T_1$ and $T^* > T_1$.

In view of real chemical kinetic mechanisms, mathematical simulation methods should be invoked for a more detailed theoretical analysis of the emergence of one or another regime of combustion wave propagation. We will consider the classical one-dimensional formulation of the problem on combustion wave initiation in a combustible gaseous mixture for a given initial linear temperature gradient [7, 9]. The initial conditions for $t = 0$ define the temperature gradient in the immobile combustible mixture at a constant pressure:

$$T(x,0) = T^* - \frac{(T^* - T_0)x}{L}\,, \qquad 0 < x < L\,, \tag{2}$$

$$p(x,0) = p_0\,, \tag{3}$$

$$u(x,0) = 0\,. \tag{4}$$

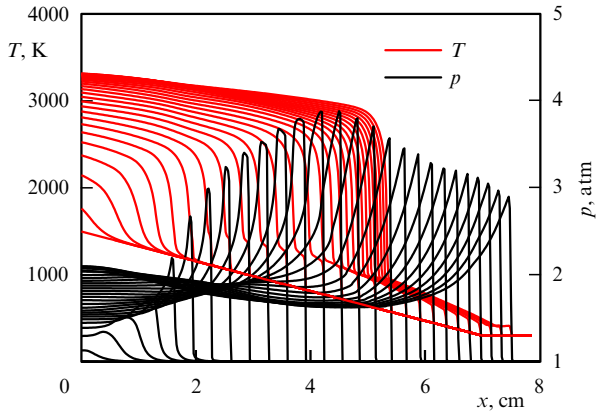

Figure 1. (Color online.) Spontaneous combustion wave travels along a temperature gradient and generates a pressure wave behind its front; as the spontaneous combustion wave slows down, the pressure wave catches up with it and forms a shock wave when crossing its front. In this case, the spontaneous mechanism of combustion wave propagation is replaced by the gas-dynamic one in the flow behind the front of the outgoing shock wave. The evolution of temperature (red curves) and pressure (black curves) profiles is given for combustion wave initiation in a hydrogen-oxygen mixture for $a_{\rm f} < \min U_{\rm sp} < a^*$ and a temperature gradient with $L = 7$ cm, $T_0 = 300$ K, and $T^* = 1500$ K. The profiles are spaced with time intervals of 2 μs.

The left boundary, $x = 0$, is assumed to be a solid adiabatic wall, at which the initial temperature is highest, $T(0,0) = T^*$. The temperature nonuniformity (gradient) is characterized by the maximal temperature T^*, the background temperature T_0, and the temperature gradient length scale L. The mathematical model includes the complete system of Navier–Stokes equations for a viscous compressible medium with the inclusion of thermal conduction, multicomponent diffusion, real equations of state, and kinetics of the chemical oxidation reaction. The system of equations was numerically solved using a Lagrangian–Eulerian method. The correctness of the results was provided by selecting a sufficiently fine spatial grid and was verified by comparing the test simulation data with the data of physical experiments.

At first we consider the $T^* > T_1$ case, which best approximates the ignition conditions in nature and in experiments ($T^* > 1200$ K). For sufficiently weak temperature gradients (high, supersonic, velocities $U_{\rm sp}$), the spontaneous combustion wave generates a pressure wave behind its front; as the spontaneous combustion wave slows down, the pressure wave catches up with it and forms a shock wave when crossing the spontaneous wave front in the vicinity of $T = T_1$ (Fig. 1). As this takes place, the spontaneous mechanism of combustion wave propagation is replaced by the gas-dynamic one in the flow behind the front of the outgoing shock wave. Depending on the velocity of the spontaneous reaction wave determined by the temperature gradient, different propagation modes of the resultant combustion waves may be realized at the point of its maximal deceleration in the region of $T \sim T_1$. Marked out in this case are the following characteristic velocity scales, which determine the criteria for the formation of one combustion regime or another: the sound (sonic) speed $a_{\rm CJ}$ at the Chapman–Jouguet point of stationary detonation, the sonic speed $a_{\rm N}$ at the von Neumann point, the sonic speed $a_{\rm b}$ in combustion products, the sonic speed in the unperturbed medium at the lower ($a_{\rm f} = a(T_0)$) and upper ($a^* = a(T^*)$) temperature gradient points, and the normal combustion

velocity U_f (the laminar flame velocity). Here, the number of characteristic scales is greater than in Ya B Zeldovich's modes classification based on a single-step reaction model, now making it possible to obtain a classification of resultant combustion regimes improved for the case of a detailed reaction mechanism.

(1) When $\min U_{sp} > a_{CJ}$, the resultant combustion wave, upon crossing by the shock wave, travels with a higher velocity than the sonic speed at the Chapman–Jouguet point, which determines the conditions for the locking of these two waves and the formation of a detonation complex according to the Chapman–Jouguet stationary detonation concept [6].

(2) For $a^* < \min U_{sp} < a_{CJ}$, the generated combustion wave is accelerated in the flow behind the outgoing shock wave, which causes the transition from combustion to the detonation. Two scenarios are possible in this case:

(a) for $a^* < \min U_{sp} < a_N$, the reaction wave accelerates in the flow behind the outgoing shock wave beginning from a velocity close to the local sonic speed a_b (for characteristic ignition temperatures $1200 < T < 1500$ K $a^* \leqslant a_b$). When the reaction front velocity becomes equal to the local sonic speed, the perturbations, which are generated by the flame accelerated in the flow, are 'locked' in the reaction zone by the supersonic flow ahead of the front. This results in a super-exponential pressure increase in the reaction zone and the formation of a shock wave, which overcomes the sound barrier and triggers detonation in the fresh mixture (this mechanism was first formulated in the solution of the problem of flame acceleration in channels [20], which will be considered below). We note that at temperatures $T^* > 1500$ K the sonic speed at the upper point of the gradient is higher than the one in combustion products, $a^* > a_b$. This requires replacing — in the $a^* < \min U_{sp} < a_N$ criterion — the lower bound a^* by the sonic speed a_b in the products of combustion;

(b) for $a_N < \min U_{sp} < a_{CJ}$, a quasistationary structure forms consisting of the shock wave and the reaction zone. In the propagation down the temperature gradient, this structure transforms into a detonation wave. This mode is the natural manifestation of the relation for combustion wave velocity, $U_w > a_N$, where a_N determines the position of the detonation front, behind which the exothermal reaction begins.

(3) For $a_f < \min U_{sp} < a^*$ (see Fig. 1), no frame front acceleration to the local sonic speed occurs and there is no pressure peak formation in the reaction zone. The resultant shock wave departs forward to compress and heat the gas, through which the 'fast' combustion wave travels as an intermediate asymptotics.

(4) For $U_f < \min U_{sp} < a_f$, the pressure wave overtakes the subsonic reaction wave and travels forward in the form of a compression wave without transforming into a shock wave over the temperature gradient length scale. In this case, the reaction propagates at a nearly constant pressure in the mode of a 'fast' combustion wave, which is intermediate asymptotics with a velocity $U_w > U_f$.

(5) For $\min U_{sp} < U_f$, the heat transfer rate due to thermal conduction is higher than the spontaneous combustion wave velocity, and a deflagration wave forms, which propagates due to thermal conduction with a normal velocity $U_w = U_f$. The ignition of the combustion wave is bounded below by the minimal heating domain size whereby the rate of heat removal becomes higher than the velocity of reaction propagation due to thermal conduction.

In the earlier studies [7, 9–12] performed in the single-step kinetics approximation, heat release takes place from the very beginning and at every point of the temperature should be gradient domain, and so the gas dynamics 'start up' at once along the entire gradient. In the single-step model, the pressure wave originates not behind the spontaneous wave as in the detailed chemical model, but immediately in the whole gradient domain, including ahead of the spontaneous wave front. Consequently, gas dynamics play the decisive role from the very beginning. As a result, the dynamics of shock and detonation wave generation change (modes 1–3 in the above classification) and, as a result, the temperature gradient length required for detonation initiation changes. The single-step model gives a smaller value for this quantity than the temperature gradient length calculated according to the detailed chemical kinetics model [14, 15].

Now let us consider the case with gradient apex temperature $T^* \lesssim T_1$. As shown by numerical simulation data [15], to initiate shock and detonation wave formation modes for low temperatures in the ignition domain requires a substantially milder sloping and longer temperature gradient. In this case, the very mode formation is different from that when the gradient has a high temperature T^*. For a low temperature at the upper point of the gradient, the duration of the induction stage may be several orders of magnitude longer than for a higher temperature. However, a more significant qualitative difference is that on lowering the temperature and transiting the 'extended second ignition limit' the induction stage becomes longer than the stage of radical recombination with heat release. Prior to the formation of a stable exothermal reaction front, even at the induction stage there is moderate energy release lengthwise of the gradient domain, which forms a pressure wave with a maximum at the initial point $x = 0$ of this domain. Therefore, immediately after the beginning of exothermal reaction wave propagation along the temperature gradient domain the pressure wave overtakes it (for low temperatures $U_{sp} < a^*$) to produce a shock wave ahead of the reaction front. In this case, the intensity of the shock wave is determined by the reaction rate at point $x = 0$. The stated mode of combustion formation is similar to that realized in the case of a single-step exothermal reaction, when the decisive role is played by gas dynamics and not by Ya B Zeldovich's mechanism.

In the ignition of a gaseous mixture by localized energy sources, an important factor is the thermal explosion character variation with increasing pressure in the region of energy input. At low pressures, the high-temperature range determines the initiation conditions for a so-called nondegenerate thermal explosion, when the induction time is far shorter than the ignition time, which includes the induction time and the exothermal reaction time. On moving to temperatures below the 'extended second limit', the induction time becomes shorter than the exothermal reaction time and the ignition conditions correspond to a degenerate thermal explosion. As shown above, as regards the realization mechanism, it is closer to a single-step explosion, when the induction time does not stand out against the background of the entire ignition process. With increasing pressure, triple collisions come to prevail, which determine the exothermal radical recombination reactions in the first place. As the pressure becomes higher, the induction and ignition times shorten discordantly and the 'extended second limit' shifts to the higher temperature domain. The thermal explosion transitions into a degenerate one.

Therefore, the qualitative picture of ignition development in the low-pressure case is similar to that observed at normal pressure and a high temperature T^*. In this case, the temperature gradient length required for realizing the modes with shock and detonation waves becomes much greater and the 'velocity' bounds separating the domains of different modes are defined by the sound velocities a_0, a^*, and a_{CJ}.

By contrast, in the high-pressure case, the picture of ignition development comes to resemble the picture realized in the single-step model or for low values of T^*, which results in a lowering of the bounds for the existence of intermediate modes 2 and 3. Thus, since the induction times are much shorter for high pressures, the lengths of temperature gradients required for realizing one mode or another, in particular for the direct initiation of detonation, are also much shorter. In particular, for sufficiently high pressures, $\gtrsim 50$ atm, direct detonation initiation by the temperature gradient in hot spots of 3–5 mm in size becomes possible, which is considered in Ref. [21] as a possible mechanism for the effect of knocking in ICEs.

2.2 Initiation of combustion waves by localized thermal energy sources

In Section 2.1, proceeding from the notion of spontaneous combustion waves, it was shown how different combustion modes are formed on a nonuniform temperature background. At the same time, the very initiation of some kind of combustion mode depends on the spatio-temporal characteristics of the source of energy input. An analysis of this dependence permits making a correct estimate of the input energy and the spatial scale of its localization, and subsequently using Ya B Zeldovich's conception to describe the ignition driven by nonstationary energy sources.

The time dependence of energy input and the spatial energy localization are determined by the nature of the physical source (electric spark, laser-produced spark, heated surface, shock wave, etc.). In this case, the entire variety of sources may be divided into three groups according to the nature of action on the medium: (1) short high-energy pulses; (2) short low-energy pulses; (3) long pulses. Out of the diversity of physicochemical processes occurring under high-intensity energy input, it is possible to mark the most significant ones for the broadening of the combustion zone at the initial stage. Then the process of combustion initiation may be reduced to only a gain in internal energy (temperature) of the combustible mixture according to a prescribed time dependence in a given small spatial domain. Therefore, it is possible to restrict ourselves to the consideration of only the thermal energy sources as was assumed in Refs [22, 23]. Here, it is possible to single out four main time scales of the problem, whose ratio will determine the formation of one mode or another for the given energy input parameters: (1) the period of energy input Δt_Q; (2) the ignition time delay t_{ign}, which characterizes the duration (τ_{ind}) of the induction stage with consideration of the energy input rate; (3) the characteristic acoustic time $t_a = L/a_f$ defined by the ratio between the size of the energy input domain and the local sonic speed; (4) the characteristic thermal wave propagation time $\tau_T \sim L^2/\chi$, which depends on the thermal diffusivity χ.

It is noteworthy that ignition may occur either after the whole energy input ($t_{ign} \geqslant \Delta t_Q$) or during the energy input ($t_{ign} \leqslant \Delta t_Q$), depending on the energy input rate. In the latter case, after the ignition the energy is deposited into hot products, which hardly affects the development of the combustion mode resulting from the ignition. Therefore, of greatest interest is the consideration of the energy input modes with $\Delta t_Q \leqslant t_{ign}$. For a high energy input rate ($\Delta t_Q \ll t_a$) and a high input energy, the ignition is determined by the conditions of the thermal explosion for the temperature and pressure resulting from the energy input. For a low energy input rate ($\Delta t_Q \gg t_a$), the pressure will manage to equalize and the ignition process will proceed under the conditions of constant pressure. For moderate energy input rates and energy inputs, the ignition mode will be determined by the ratios between all indicated time scales.

A rapid energy input during the time much shorter than the characteristic acoustic time ($\Delta t_Q \leqslant t_{ign} \ll t_a$) produces a uniform increase in temperature and pressure in the energy input domain, resulting in the realization of ignition by the mechanism of volume explosion inside a 'hot spot'. In this case, the temperatures and pressures are completely determined by the amount of energy input. After the energy input and the following induction phase, initiation of a combustion or detonation wave occurs. For an energy input with the duration approaching the acoustic time ($\Delta t_Q \leqslant t_{ign} < t_a$), at the boundary between the hot spot and the unperturbed medium a discontinuity break-up occurs with the resultant formation of a compression wave, which propagates into the unperturbed medium, and a rarefaction wave, which removes energy from the hot spot volume. In the case of sufficiently strong shock formation at the hot spot boundary, this scenario, which is similar to that of the development of a strong explosion, may initiate detonation immediately behind its front. For a lower intensity of the shock wave, a more interesting scenario, shown in Fig. 2, unfolds. The time evolution of the temperature and pressure profiles in the hot spot domain ($L = 1$ cm, $t_a \sim 20$ μs) during the energy input is shown in Fig. 2a. The rarefaction wave forms gently sloping temperature and pressure gradients on a scale on the order of the hot spot size. For an atmospheric pressure, $p_0 = 1$ atm, the temperature gradient with the resultant temperature difference and a characteristic size $L = 1$ cm cannot lead to detonation [15]. However, since the pressure of the heated medium rises to ~ 4 atm in the course of energy input, this gradient gives rise up to detonation according to the Zeldovich mechanism, as is clear from Fig. 2b.

For ultrashort energy input pulses ($t_{ign} \ll t_a$), the shock wave, together with a reaction zone emerging behind its front, forms a detonation complex when the shock wave velocity is comparable to the sonic speed at the Chapman–Jouguet point of stationary detonation or exceeds it ($U_{SW} \geqslant a_{CJ}$) at the instant the shock emerges from the domain of energy input. For longer ($t_{ign} < t_a$) and lower-intensity pulses, in the ignition zone on the resultant weak descending gradient, in accordance with Ya B Zeldovich's mechanism, a supersonic spontaneous combustion wave develops: the formation of detonation following the same scenario shown in Fig. 2b. In the case of a sufficiently weak (shallow) gradient, the velocity of a spontaneous wave at the point of its maximum deceleration exceeds the sonic speed at the Chapman–Jouguet point, $\min U_{sp} > a_{CJ}$, which determines the velocities of the shock and combustion waves generated at this point, the combustion wave transitioning into detonation. In the neighborhood of the detonation limit, it is possible to experimentally observe the formation of detonation propagating in an 'overdriven' mode defined by heightened parameter values ($U_D > U_{CJ}$, $p_{CJ} > p_{CJ,0}$, $a_{CJ} > a_{CJ,0}$) [26]. Figure 3 shows the chronograms of the

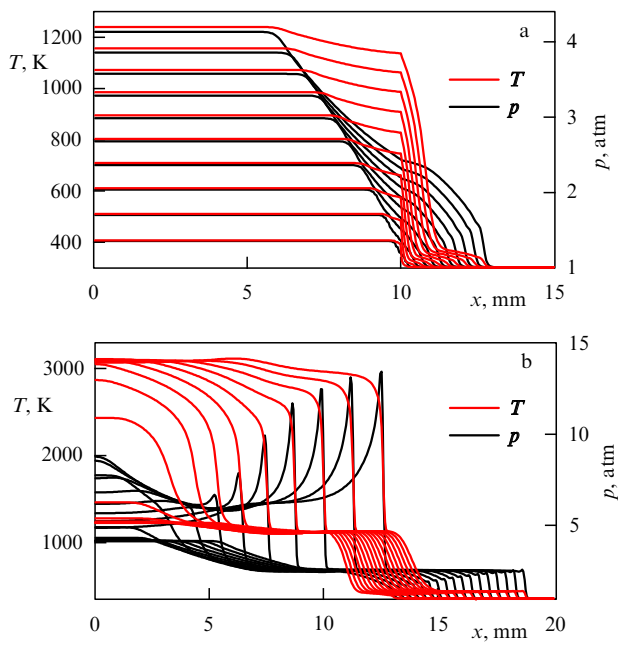

Figure 2. (Color online.) Detonation initiation by a short high-energy pulse proceeds in two stages: (a) at the boundary between the hot spot and the unperturbed medium a discontinuity decay occurs, with the resultant formation of a compression wave, which propagates into the unperturbed medium, and an rarefaction wave, which forms weak temperature and pressure gradients on the scale of the order of the hot spot size; (b) detonation is formed on the resultant gradient according to Ya B Zel'dovich's mechanism. The temperature (red curves) and pressure (black curves) profiles in the detonation wave initiation in a hydrogen-oxygen mixture by a localized energy source, $L = 1$ cm, $\Delta\tau_Q = 5$ μs, are spaced with time intervals of 0.5 μs.

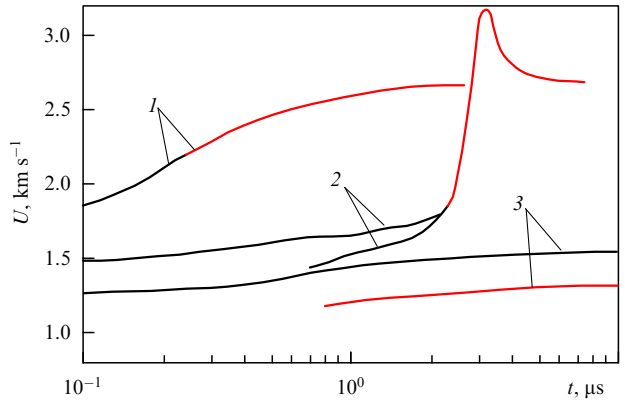

Figure 3. (Color online.) In the case of ultrashort energy pulses, the initiation of one or another combustion mode is determined by the intensity of the shock wave produced in the domain of energy input: for $U_{SW} \geqslant a_{CJ}$ a detonation forms (*1*); for a lower shock intensity, a combustion wave propagates in the flow behind its front accelerating up to transition into a detonation (*2*) or propagate in a fast deflagration mode (*3*). Chronograms of reaction waves velocities (red lines) and shock wave velocities (black lines) are shown for ignition by a submicrosecond ($\Delta\tau_Q = 0.1$ μs) energy pulse localized in a domain with $L = 1$ mm.

velocities of the shock wave (SW) and the reaction wave (RW) in three cases: direct initiation of a stationary detonation (*1*), formation of an overdriven detonation (*2*), and formation of slow combustion (*3*).

When a lower energy is input under the same conditions, the ignition time may turn out to be longer than the acoustic time ($\Delta t_Q < t_a < t_{ign}$), and the rarefaction wave will form the gradient after the energy input at the induction stage. During the longer induction stage, acoustic perturbations equalize the pressure in the domain of energy input, and ignition takes place on a stationary temperature gradient at a constant pressure. When the energy input period is somewhat longer than the characteristic acoustic time ($t_a < \Delta t_Q < t_{ign}$), the rarefaction wave manages to reach the epicenter of the hot spot and reflects from it. As a result, a nonuniform temperature distribution develops with two oppositely directed gradients: a weak gradient directed towards the interior of the hot spot and an oppositely directed strong gradient. In this case, the steep gradient directed towards the unperturbed domain is capable of producing only a combustion wave, while the weak gradient directed towards the center of the hot spot is able to initiate detonation.

The modes of combustion initiation by short high-power energy-input pulses considered above are significantly different from the modes of combustion initiation by long low-power pulses ($t_a \ll \Delta t_Q < t_{ign}$). During the energy input time, acoustic perturbations manage to equalize the pressure in the domain of energy input. Then, no strong shock waves are generated and the resultant combustion mode is determined only by the degree of flatness of the temperature gradient formed due to the gas-dynamic expansion of the hot spot and the propagation of the thermal wave. The extent of the thermal gradient domain turns out to be greater than the scale length of thermal wave propagation domain, which is largely attributable to the broadening of the hot spot owing to density decrease in the course of energy input. According to Ref. [15], the resultant gradient is insufficiently weak to initiate detonation according to Ya B Zeldovich's mechanism. The heat propagation in the medium and the heated gas expansion turn out to be too slow to form the temperature gradient sufficient for initiating detonation on the energy input time scale. Long before the thermal wave travels a sufficiently long distance, the temperature at the epicenter of the hot spot reaches a value required for ignition, which gives rise to a combustion wave on the temperature gradient formed by this moment. We note that, according to the criteria obtained in Ref. [15], to initiate detonation at a heightened pressure requires a substantially steeper (less extended) temperature gradient than at atmospheric pressure or a lower one. Therefore, at increased pressure it becomes possible to produce detonation by long low-power energy-input pulses.

Although the presented results are mostly qualitative in character, they may be used for estimating the energy required to initiate some type of combustion mode. In this case, the shorter the energy input period in comparison with the characteristic acoustic time ($\Delta t_Q < t_a$), the less significant the role played by the dimensional factor. The role of the rarefaction wave in the formation of the combustion mode becomes less significant in this case, as shown in Ref. [23], whose results agree nicely with the lower bound of detonation initiation in hydrogen determined experimentally.

The above brief analysis of nonstationary combustion processes suggests there are two main initiation mechanisms of reaction waves, depending on the energy input parameters (the input energy and the duration and size of the domain of energy input): Ya B Zeldovich's gradient mechanism and the volume thermal explosion, which is one of the asymptotics of this mechanism for a zero-slope gradient. Therefore, Ya B Zeldovich's mechanism is the most general one for

describing the physical picture of ignition of combustible gases.

2.3 Inflammation near concentration limits

Another important application of Ya B Zeldovich's theory of the formation and propagation of exothermal reaction waves in media with a nonuniform reaction-time distribution is the determining of the concentration limits of ignition and stable combustion. This problem became especially urgent in connection with the ruinous hydrogen explosions in serious accidents in NPPs.

We consider the most crucial criterion in the solution of explosion safety problems — the lean limit of combustion. The properties of combustion of a lean hydrogen-air mixture were determined primarily in experiments: the value of the lean ignition limit was obtained back in 1952 in Ref. [24], according to which this limit, under normal conditions (the temperature of a fresh mixture $T_0 = 300$ K, the density $p_0 = 0.1$ MPa), is $[H_2]_{min} = 4.1\%$ volume of hydrogen (molar fraction). At present, this value of the lean concentration limit is commonly recognized and is cited in fundamental monographs and reviews (see, for instance, Ref. [25]). This value is, in fact, the result of a general convention, while in real physical experiments this lean limit is directly dependent on measurement conditions and is different from the conventional 4%.

In most experimental work, as a rule, additional calculations of adiabatic equilibrium pressure at constant volume have been made to interpret the results. Agreement between the measured and calculated pressure values permitted determining the concentration limit for which combustion enveloped the entire chamber volume. This mode was observed for a volume hydrogen concentration of 10% and above. For a lower hydrogen content in the mixture, the calculated and measured pressure values diverged considerably. This comes as no surprise, because the process was not equilibrium for a hydrogen content of less than 10%, as shown by experiments. To obtain a more detailed picture of the ignition of hydrogen-air mixtures, calculations were made of the combustion of lean mixtures using the complete system of equations of combustion gas dynamics.

The main factors which determine the inflammation threshold are the characteristic time scales of the induction and exothermal stages of combustible mixture ignition. At the same time, the mixture ignition requires an additional extraneous energy input. The relative contribution of this energy input to the energy characteristics and dynamics of the medium may be rather large for lean mixtures, which can change the value of the inflammation threshold.

To rule out extraneous effects, the problem of the ignition of a hydrogen-air mixture will be considered in a formulation similar to that of the classical Ya B Zeldovich problem of the development of a spontaneous ignition wave on the gradient of induction time (in our case, on the gradient of hydrogen concentration). We note that the approach under consideration may also be applied to any other combustible gaseous mixtures, whose concentration limits of ignition have not infrequently been less well studied than for hydrogen mixtures. Depending on the volume fraction of the combustible component in the mixture, the initiation of combustion, i.e., the accumulation of the necessary number of radicals with their subsequent recombination and energy release, proceeds on different time scales. Therefore, for a given constant temperature at which a stoichiometric mixture is

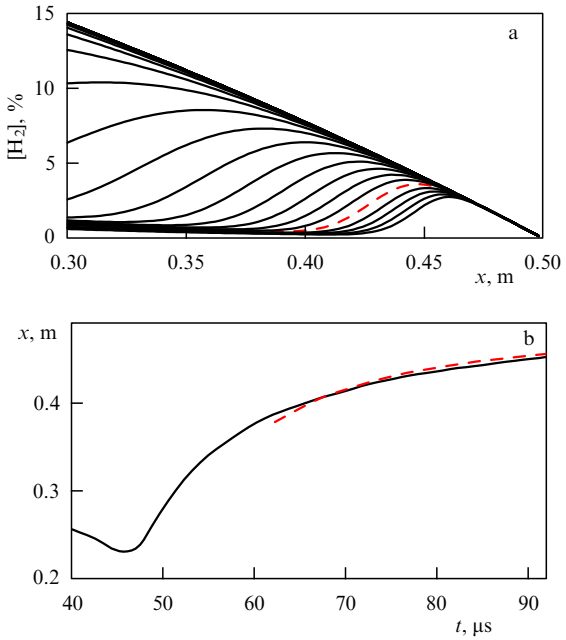

Figure 4. The existence of a spontaneous combustion wave on the concentration gradient is limited by concentration limits of ignition; as they are approached, the wave decelerates to generate a compression wave, which overtakes the front of the reaction wave and determines the dynamics of the process at a later stage. (a) Evolution of $[H_2]$ concentration profiles in the course of ignition. The profiles are spaced with time intervals of 2.5 μs. The dashed curve shows the profile which defines the ignition limit. (b) Trajectories of the front of the exothermal reaction wave (solid curve) and the compression wave generated by the spontaneous wave at the stage preceding its degeneracy.

expected to inflame, it is possible to prescribe the spatially nonuniform distribution (the gradient) of hydrogen concentration (which is equivalent to the gradient of induction time in this case) on which a spontaneous combustion wave may form, in accordance with Ya B Zeldovich's mechanism, to propagate from the point with the minimal induction time towards the point with the maximal induction time. At the point where the induction time ceases to be distinguishable against the background of ignition time, the role of the diffusion mechanism comes to dominate, the spontaneous wave ceases to exist, and the temperature wave propagates due to thermal conduction and diffusion. This point may be considered as the concentration limit of ignition. In the classical formulation of the problem on the ignition on a temperature gradient, the limit for the existence of a spontaneous wave is defined by the condition $U_{sp} < U_f$. When $U_{sp} < U_f$, the spontaneous wave travels more slowly than the combustion wave, which propagates with normal velocity U_f, so that diffusion processes proceed faster and, therefore, the ignition according to the spontaneous mechanism is not realized.

Calculations of the development of a spontaneous combustion wave over the hydrogen concentration gradient were carried out under the following initial conditions: the hydrogen-air mixture composition varied along the domain of concentration gradient from the stoichiometric one to pure air, in which the hydrogen concentration was equal to zero. The initial temperature was equal to 1200 K and the extent of the gradient domain was 0.5 m. The results of the calculations are shown in Fig. 4. Naturally, the resultant picture is significantly different from the one corresponding to the

temperature gradient and invites additional explanation. The ignition reaction begins independently at each point of the gradient domain; in this case, the induction stage proceeds rather slowly in the hydrogen-air mixture at the selected temperature (for the stoichiometric mixture composition $\tau_{ind} \sim 40-60$ μs) and is attended by an insignificant conversion of the combustible component to combustion products. The exothermal stage begins with the release of a large amount of energy due to the nearly complete combustion of the combustible mixture. As a result, the hydrogen concentration profile in the selected formulation of the problem assumes a dome shape with time; on the right slope of this dome (heading from left to right) an endothermal reaction wave propagates, followed by an exothermal reaction wave, which determines the left slope of the dome. At a certain point in time, the spontaneous mechanism of reaction wave propagation is replaced by the diffusion mechanism; the thermal front, which is generated by the exothermal wave and which propagates due to thermal conduction and expansion of hot products, overtakes the spontaneous wave front. In the domain with a still lower hydrogen concentration, the combustion wave decays, and the subsequent evolution of the hydrogen concentration profile, which is now no longer related to the exothermal reaction, is determined primarily by diffusion and the gas-dynamic action of the expanding combustion products.

The change of modes described above is easily seen in Fig. 4: from Fig. 4b it is easy to determine the moment the compression wave overtakes the spontaneous reaction wave, and in Fig. 4a it is possible to mark out the density distribution curve at the given point in time and determine its corresponding value in the concentration gradient. In the problem under consideration, this value is equal to 4.2% of hydrogen in the initial combustible mixture composition.

The resultant hydrogen concentration threshold defines the limit below which the chemical composition of the mixture does not sustain the progress of the exothermal reaction. In this case, a gradual increase in combustible component concentration does not entail the immediate settling of a stable combustion mode, which is settled only when the hydrogen concentration overcomes some unstable combustion interval. According to experimental data and numerical simulations, this takes place when the concentration reaches the threshold of about 10%, which may be treated as the limit which ensures the stable combustion of a uniform mixture. (In several fire safety instructions, this is precisely the pattern which is taken for the lean density limit for the ignition of a hydrogen-air mixture in technogenic accidents.) We note that the well-substantiated determination of the ignition limits for well-mixed compositions becomes less evident for unmixed compositions with a nonuniform spatial distribution of the mixture components. Figure 5 shows the temperature variation behind a wave front propagating from the domain of energy input for lean hydrogen-air mixtures.

The additional increase in temperature in the energy input zone due to chemical reactions obtained numerically does not signify that such ignition event will directly give rise to a self-sustaining combustion wave propagating through a mixture of a given composition. As may be seen from Fig. 5, for the uniformly mixed lean hydrogen-air mixtures considered, a stable reaction wave is not formed and the combustion emerging at an early stage gradually decays or exhibits an unstable behavior, periodically blazing up and decaying. (The last phenomenon was observed for a hydrogen concentration above 8% over a time longer than in Fig. 5.) For a mixture with a nonuniform hydrogen concentration, a self-sustaining flame propagation mode emerges in all considered variants. The temperature is seen to rise and reach the level corresponding to the temperature of combustion products in a 15% hydrogen-air mixture. Therefore, the energy input even in the domain with a combustible component concentration below the stable energy input level may generate a thermal wave. In the presence of a positive gradient of this concentration, this wave is able to excite a stable combustion wave in the regions with a heightened combustible component concentration. The inclusion of this factor may be of significance in estimating the fire hazard in media with a lower volume-average combustible component concentration than the threshold of stable combustion or even the lean density limit.

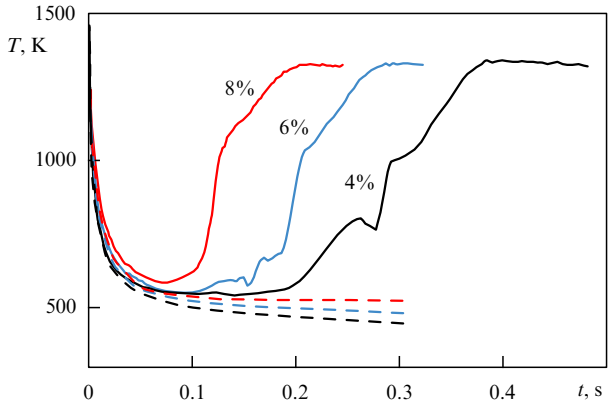

Figure 5. Results of numerical simulations of thermal wave propagation from the region of local ignition. The combustion was initiated in a 2-cm-thick layer uniformly heated to a temperature of 1500 K. The hydrogen density in this region was taken to be uniform and was specified in the range between 4% and 8%. Outside of the energy input region, either the same hydrogen concentration was retained or a linear increase in hydrogen density up to 15% over a length of 1 cm was prescribed at the boundary of this region. Shown are the temperatures behind the diffusion wave front for the uniform concentration distribution (dashed curves) and behind the reaction wave front in the case of concentration gradient (solid curves) for different values of hydrogen density (%) in the region of energy input.

3. Flame acceleration and transition to detonation in channels

For many years, one of the most demanded uses of Ya B Zeldovich's spontaneous wave conception was its application to the solution to the problem of transition from slow combustion to detonation [10–14]. The results obtained by Ya B Zeldovich were used to construct the theories of detonation formation in channels and tubes, which rely on the possible formation of self-ignition conditions ahead of the flame front. The theory of shock wave amplification by coherent energy release (SWACER) [26] and the theory of self-ignition in hot spots [27, 28] have received the widest acceptance. Owing to the limitations of experimental methods, which permit reconstructing the combustion dynamics in channels only from side channel surface data (from pressure sensors and soot imprints) and the flow structure data obtained with the use of interference schlieren photography, there is no way of obtaining a reliable experimental verification of the constructed theories. To date, these theories have

been practically borne out only by numerical simulations of the process using a simplified single-step kinetic model, which does not take into account the existence of the endothermal stage of mixture component decomposition and radical accumulation preceding the exothermal stage of their recombination. Evidently overlooked under this simplification are the special features of ignition at relatively low temperatures ahead of the flame front, in the region which must be embraced by the theories under elaboration. In particular, such detonation initiation modes were not observed in the latest work on the numerical simulation of combustion and transition to detonation for hydrogen-based mixtures with the use of detailed combustion kinetic models [20, 29]. In the numerical simulation, the self-ignition ahead of the flame front emerged only in the case of complex interference of shock waves in an enclosed volume, which is not realized in natural experiments performed to investigate the flame acceleration and transition to detonation in long (semi-open) channels in the absence of external action.

On the other hand, the transition to detonation is a direct consequence of flame acceleration in a channel, and it is therefore natural to assume that it is precisely the dynamics of a nonstationary accelerating flame which should determine the conditions for detonation formation. In 1947, Ya B Zeldovich [31] performed a comprehensive analysis of the problem of flame acceleration in a semi-open channel with flame initiation at the closed end in view of K I Shchelkin's experimental results. Ya B Zeldovich derived the characteristic relaxation times of the laminar and turbulent velocity profiles and the characteristic time of heat exchange with the channel walls. He showed that the flame stretching in an essentially nonuniform flow is the main flame acceleration factor among the specified ones. In this case, turbulence plays only a subsidiary role. The initially present turbulence merely favors a faster settling of the velocity profile and, as a consequence, a faster settling of the accelerating flame propagation mode. At the same time, the flow turbulization, which is caused by the flow ahead of the flame front itself, develops on a rather long time scale. Specifically, for highly reactive mixtures like hydrogen-oxygen ones this time scale exceeds the duration of the flame acceleration process up to the transition to detonation.

Therefore, the flow turbulization ahead of the flame front is not the decisive factor determining the flame acceleration and transition to detonation, at least for highly reactive mixtures. The flow turbulization becomes the decisive factor in the flame propagation in large and abstracted volumes. On a large scale, the acceleration of a freely accelerating flame is determined primarily by the development of hydrodynamic flame front instabilities, which result in only a low flame acceleration in comparison with the acceleration caused by the flame stretching in its motion through relatively narrow channels. On the other hand, the development of instabilities of this kind has the effect that the front becomes significantly distorted and acquires a fractal structure [32, 33]. This, in turn, may give rise to local flow turbulization near the flame front with subsequent downstream perturbation propagation, which may supposedly be an additional factor of flame acceleration due to the turbulization of the medium. In an obstructed volume, the state of developed turbulence may be reached even prior to the flame arrival at this volume due to the interaction of the flow and compression waves with obstacles.

This effect of obstructed space on the flow in a natural experiment can be modeled by introducing turbulence stimulators (a system of obstacles) located along the detonation tube, which was widely used by K I Shchelkin in experiments to investigate the turbulence effect on the acceleration of deflagration-to-detonation transition [34, 35] and nowadays is used by researchers and developers in the area of promising detonation engines. Ya B Zeldovich [31] also estimated the external turbulence factor influence on the deflagration-to-detonation transition and showed that the presence of turbulent pulsations speeds up the development of a nonuniform flow velocity profile — the main factor determining flame acceleration.

In recent work on the numerical simulation of flame acceleration in channels and transition to detonation in a hydrogen-oxygen mixture, the laminar flow structure in the vicinity of the flame front was confirmed to exist up to the transition to detonation. Figure 6 shows accelerated propagation of the three-dimensional surface of the flame front in a channel filled with a hydrogen-oxygen mixture; these three-dimensional computer simulations were made on the basis of the complete Navier–Stokes equations with the inclusion of thermal conduction, multicomponent diffusion, and chemical transformations in the reaction zone [36]. One can see that the initially unperturbed flow retains its laminar structure in the course of evolution and flame acceleration up to the instant of detonation formation. In this case, the shadow photographs constructed on the basis of three-dimensional simulations (Figs 7a, 7b, 7d, and 7e) reproduce rather well all the features of the images obtained experimentally in Ref. [37] (Figs 7c and 7f). The shadow visualization of the flow exhibits a rather complex flow structure due to the interference of separate unrelated parts of the flame front surface. Therefore, it may be assumed that the conclusions about the turbulent flow structure near the flame front, which were drawn in the analysis of experiments in several papers, may well be an artifact of the diagnostic techniques, which do not provide a correct reproduction of the three-dimensional flow pattern.

Now we consider the characteristics of flame acceleration in a channel and their ensuing condition for the transition to detonation. From the instant of combustible mixture inflammation, the flame propagation dynamics evolves in several stages, which are observed in physical laboratory experiments and reproduced in computational experiments [20, 29]. At the first stage, the flame front dynamics are determined by the expansion of combustion products, which force out the flame front from the ignition zone. Next, owing to a nonuniform mass velocity distribution over the channel section, the surface of the flame front increases and expands in the flow. This leads to an increase in total inflow of the fresh fuel to the front and thereby increases the velocity of flame propagation observed at the second stage of the process. Here, the growth of velocity may be described by an exponential dependence, which reflects the feedback between the acceleration of the flame front and the flow acceleration ahead of it [20]. As the process develops, it enters the third stage, during which the front surface completely adjusts to the velocity profile in the flow and its structure stabilizes, which determines the lowering of the velocity growth rate. At this stage, the flame acceleration may be described by a power law with an exponent n, with $0 < n < 1$ [20, 29]. We note that both the exponential and power-law acceleration stages are observed in channels of width H much greater than the flame front width L_f, $H \gg L_f$ [37, 38], while in narrow channels of a width

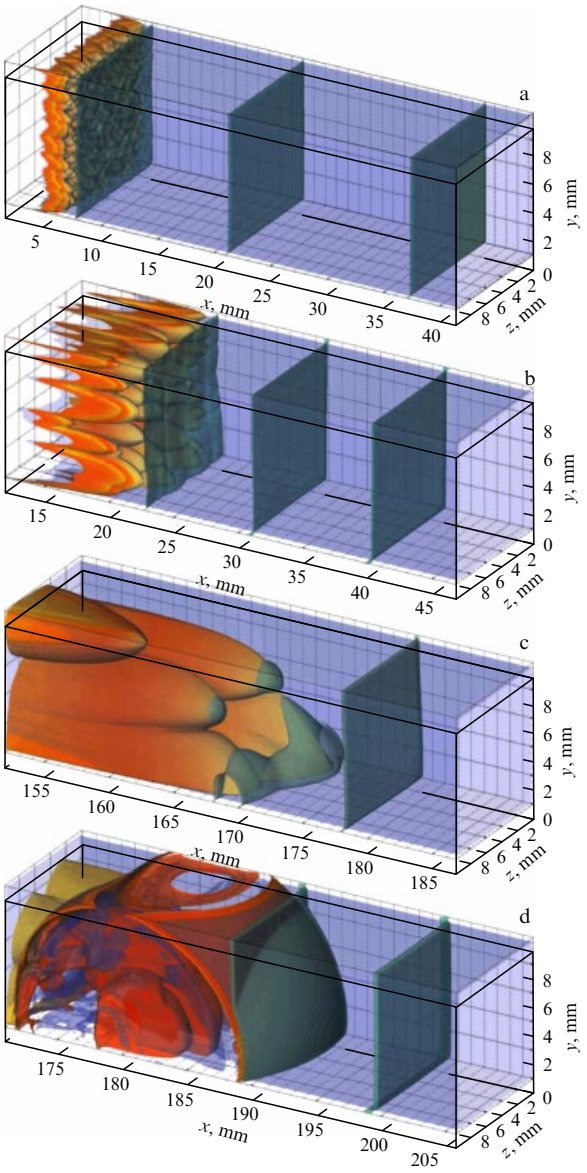

Figure 6. (Color online.) Flame acceleration in a channel filled with a combustible mixture undergoes four main stages determined by different physical mechanisms: (a) expansion of combustion products from the ignition region; (b) exponential flame acceleration in the gas flow set in motion by the flame itself; (c) acceleration according to a power law due to extension in the flow and generation of shock waves in the immediate vicinity of the flame front; (d) formation of detonation and propagation of combustion wave in the detonation mode.

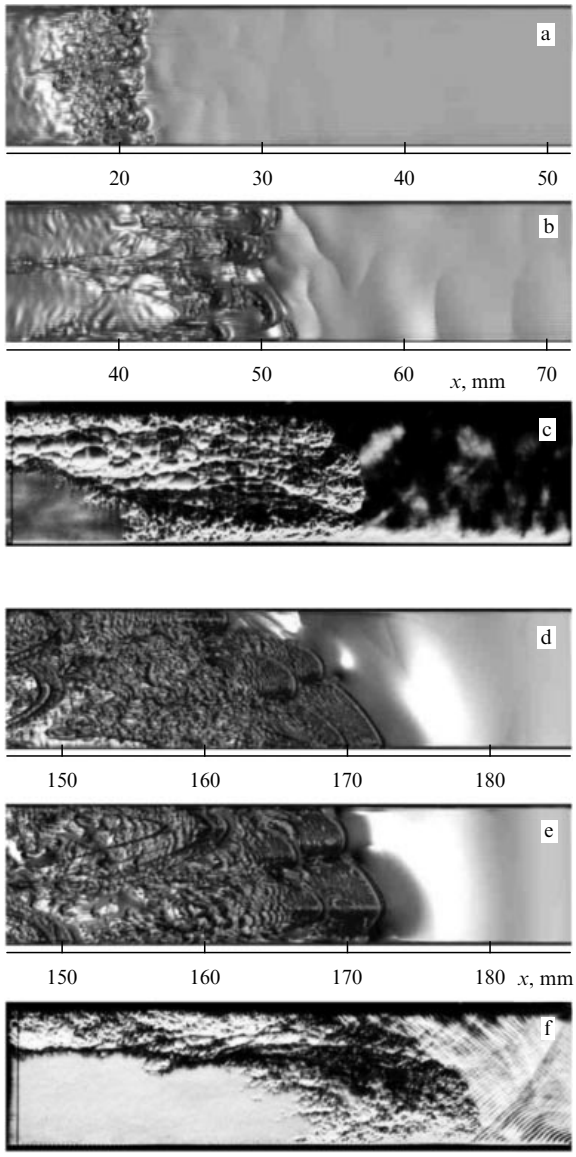

Figure 7. With the use of shadow visualization in numerical simulations (a, b, d, e) and experiment (c, f), the flow structure appears as a rather complicated picture due to the interference of separate unrelated parts of the flame front surface. The shadow visualization of the flow near the flame front surface in a square channel is shown at the stages of exponential (a–c) and power-law (d–f) acceleration.

of about the flame front width ($H \sim L_f$), the transition to detonation proceeds at the exponential stage omitting the stage of power-law velocity increase [39].

The compression waves emitted by the accelerating flame front, similarly to the compression waves generated by an accelerating piston, produce shock waves, according to Riemann's solution, at some distance from the flame front surface. At the stage of exponential acceleration, the shock wave forms at a distance of several channel widths ($X_{SW} - X_f \sim H$; X_{SW} and X_f are respectively shock wave and flame front positions), while at the stage of power-law growth with $0 < n < 1$, it forms in the immediate vicinity of the flame front surface ($X_{SW} \sim X_f \pm L_f$).

In wide channels, at the stage of power-law velocity growth, the shock waves produced immediately at the flame front deliver to the front a more compressed and heated combustible mixture, which in turn leads to a pressure increase in the reaction zone (Fig. 8). Thus, an additional reaction acceleration and an additional increase in combustion wave velocity appear. A similar effect is also observed in narrow channels, where shock waves are formed in the immediate vicinity of the front ($X_{SW} - X_f \sim H \sim L_f \Leftrightarrow X_{SW} \sim X_f \pm L_f$), even at the stage of exponential velocity growth. Consequently, the additionally compressed and heated mixture enters the flame front even at this stage. As a result of this interaction of the flame with the generated shock waves, a self-sustaining flame acceleration mode sets in both cases. As the flame accelerates, the flow ahead of the flame front is accelerated by the outgoing shock waves. When the flow velocity amounts to about the sound speed in the front,

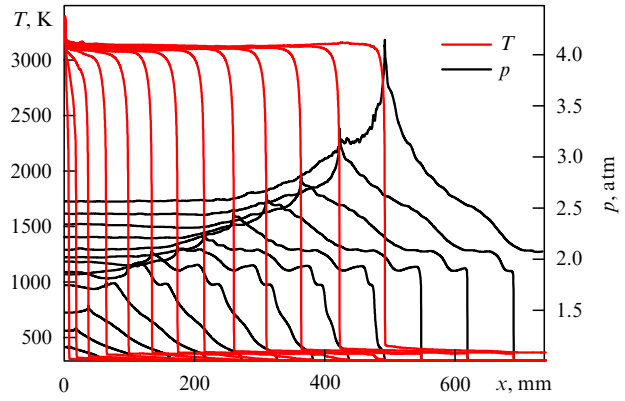

Figure 8. At the stage of power-law velocity growth with exponent $0 < n < 1$, shock waves are generated by compression waves generated by the flame front in the immediate vicinity of the flame front surface, with the effect that a more compressed and heated combustible mixture is delivered to the front, which in turn gives rise to a pressure increase in the reaction zone. This may be observed in pressure profiles as the formation of a local peak traveling simultaneously with the flame front. The temperature and pressure profiles are spaced with time intervals of 50 μs.

the compression waves generated by the accelerating flame are locked in the reaction zone by the supersonic flow. This gives rise to a violent increase in flame velocity and pressure in the reaction zone, with the resultant escape of a strong shock wave from the reaction zone, whose parameters permit overcoming the sound barrier ($U_{SW} > a_b \sim a_{CJ}$). It is this shock wave that forms detonation. In this case, the detonation formation mechanism is similar to the one discussed above in the consideration of the problem of detonation initiation in near-critical conditions, with the exception that here the mechanism of transition to detonation is not determined by the characteristics of energy input, but is triggered by the development of a transient three-dimensional process.

4. Production of nitrogen oxides in heated air

When discussing Ya B Zeldovich's enormous contribution to the theory of combustion and detonation, there is no escape from mentioning his fundamental work (made in co-authorship with P Ya Sadovnikov and D A Frank-Kamenetskii) on the physics and chemistry of nitrogen oxide production in hot air, which is efficiently produced, for instance, in combustion and behind the shock front in chemical explosions [40–42], especially so in view of the fact that Ya B Zeldovich's work on combustion and detonation is a natural continuation of his earlier work on nitrogen oxides (which dates back to the 1930s). It was precisely the study of nitrogen oxidation that formed the basis of Ya B Zeldovich's doctoral thesis, which he defended in 1939 at the age of only 25. The thesis was similarly entitled "Oxidation of nitrogen in combustion" [43]. The kinetics of thermal nitrogen oxide production proposed in these studies (which have long become classical) are deservedly referred to as the Zeldovich mechanism and are still widely used in various fields of physics, including atmospheric photochemistry, the physics of ICEs, and the physics of explosions, combustion, and detonation considered above, as well as in plasma medicine. Here, we enlarge on only one application of the indicated approach of Zeldovich et al. and consider the formation of NO_x nitrogen oxides (NO, NO_2, NO_3, N_2O_5, etc.) in the hot air of a lightning channel produced by a lightning discharge (by analogy with Ref. [41], which considered the production of NO_x in combustion).

The NO_x nitrogen oxides play one of the key roles in the photochemistry of our atmosphere; in particular, they are one of the factors determining the amount of tropospheric and stratospheric ozone, O_3, in the atmosphere. Recall that the role of stratospheric ozone is unique: it protects the biosphere of Earth from biologically harmful ultraviolet solar radiation. Furthermore, removal of nitrogen oxides from the atmosphere by way of atmospheric precipitation is one of important mechanisms of binding nitrogen required for the existence of the biosphere. The German chemist von Liebig was supposedly the first (even early in the 19th century) to draw attention to the fact that lightning discharges may be the global source of nitrogen oxides [44]. Since then, this question has been repeatedly considered, and in the scope of this review it is impossible to give a comprehensive bibliography concerning this subject; we only mention the pioneering work [45–49], in which the leading part is played by the thermal NO_x formation mechanism (the Zeldovich mechanism). In the framework of the Zeldovich mechanism, the thermal dissociation of molecular nitrogen N_2 and oxygen O_2 results in the production of N and O atoms; produced in the subsequent catalytic reactions $N + O_2 = NO + O$ and $O + N_2 = NO + N$ is nitrogen oxide, NO. The subsequent chain of chemical transformations in the hot air gives rise to the remaining NO_x nitrogen oxides. We note that tropospheric NO_x nitrogen oxides result in the production or annihilation of ozone, depending on their concentration. An excess of nitrogen oxide in the stratosphere results in the catalytic destroy of ozone molecules in the reactions $NO + O_3 \to NO_2 + O_2$, $NO_2 + O \to NO + O_2$, thereby depleting the ozone layer [50–53]. Nowadays, it is believed that lightning discharges are an important source of nitrogen oxides in the atmosphere: their contribution to the global production of NO_x is estimated in the range of 3–20% of the total nitrogen oxide production (a substantial part of the nitrogen oxide is produced by the biosphere). This amounts to about $10^{12} - 10^{13}$ g yr^{-1} (see, for instance, Ref. [54]). According to long-term optical satellite observations, the frequency of lightning discharges in the terrestrial atmosphere is $\sim 10^9$ yr^{-1}. The global distribution of lightning discharges on our planet averaged over several years is plotted in Fig. 9 (shown is the lightning flash density n_{lig} — the number of discharges per km^2 per year) [55]. It is clearly seen that the lightning flash density is highest in the subequatorial tropical regions and is insignificant above the ocean surface.

The amount of NO (as the most important compound of NO_x) produced in a lightning discharge may be estimated from simple considerations: the characteristic cooling time τ_c of a lightning channel in its expansion is equated with the characteristic time τ_{NO} of NO loss in chemical reactions in the hot air:[1]

$$\tau_c \approx \tau_{NO} . \qquad (5)$$

A very sharp increase in $\tau_{NO}(T)$ with a decrease in gas temperature T [$\tau_{NO}(T) = L^{-1}(T) \propto \exp(E_D/T)$, where $L(T)$ describes the annihilation of nitrogen oxide in chemical reactions [56], the dissociation potential $E_D \gg T$] permits

[1] For simplicity, below we restrict ourselves to the consideration of nitrogen oxidation kinetics in a lightning discharge in the case of dry air; different chemical reactions arising from the presence of hydrogenous compounds [for instance, water (H_2O), atomic hydrogen (H), hydroxyl (OH), nitric acid (HNO_3)] are not considered.

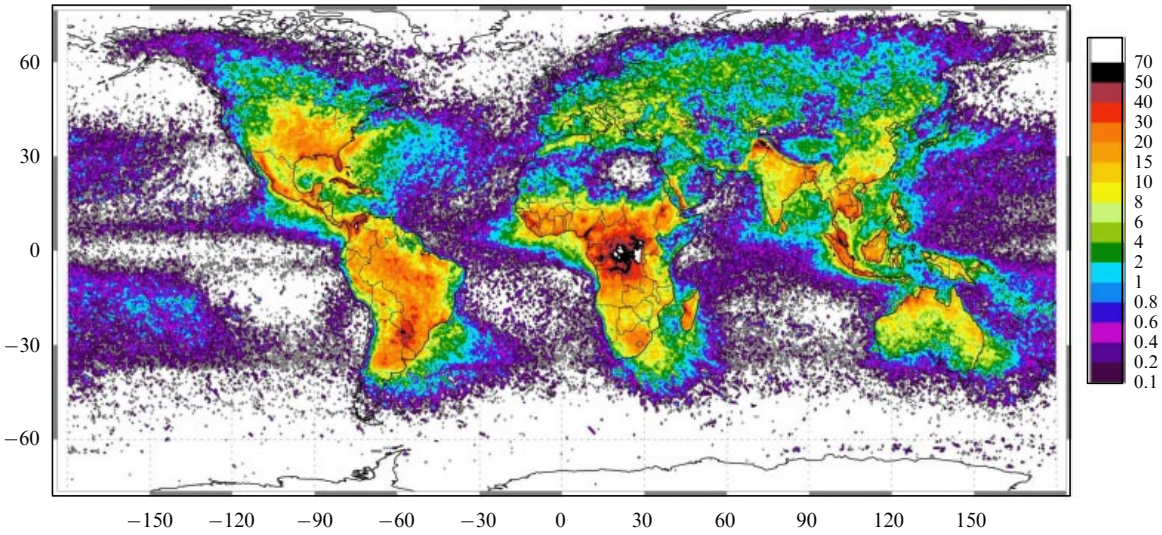

Figure 9. (Color online.) Annual distribution of lightning discharges on our planet (the number of discharges per km^2 per year) [52]. One can see that the lightning flash density n_{lig} varies over wide limits: from $n_{\text{lig}} \sim 100$ in subequatorial regions to $n_{\text{lig}} \sim 0.1$ above the ocean surface, where lightning activity is hardly present.

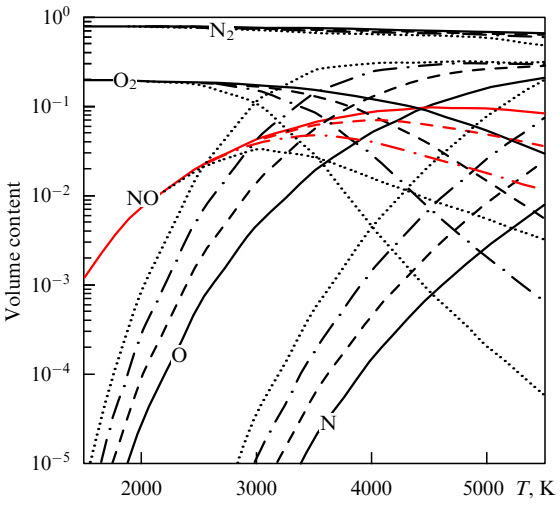

Figure 10. (Color online.) Thermodynamically equilibrium composition of heated air as a function of its temperature at different pressures: 100 bar (solid curves), 10 bar (dashed curves), 1 bar (dashed-dotted curves), 0.1 bar (dotted curves). Shown are the temperature dependences of the volume content of molecular nitrogen, N_2, molecular oxygen, O_2, nitrogen oxide, NO (the curves marked in red), atomic nitrogen, and oxygen in the hot air. One can see that the highest content, $n_{\text{NO}} \approx 0.1$, is observed at hot air temperatures $T \approx 3000-4500$ K (for the indicated pressures), which are much lower than the characteristic initial temperatures of a lightning channel generated by a return stroke ($T \simeq (1-3) \times 10^4$ K).

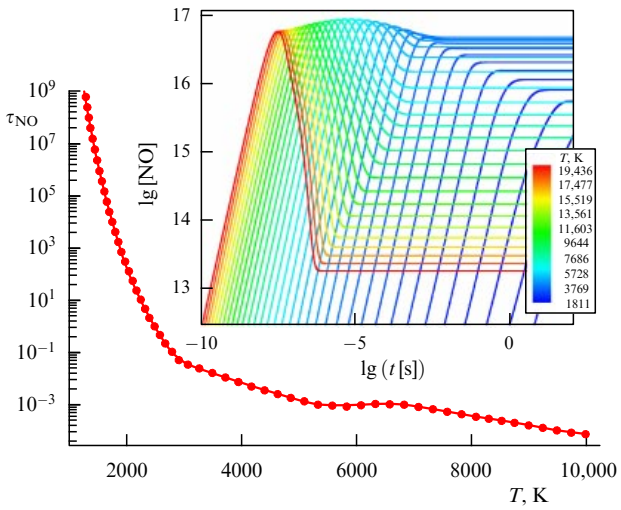

Figure 11. (Color online.) Kinetics of NO production in hot dry air. The characteristic equilibration time τ_{NO} of the thermodynamically equilibrium density of nitrogen oxide in the heated air is plotted as a function of its temperature T. The air density $\rho_a \approx 10^{-4}$ g cm^{-3}. The inset shows the NO production kinetics at different temperatures [the curves are by color-coded according to the value of T, which increases from blue to red to embrace a broad temperature range: $T \approx (0.15-2) \times 10^4$ K]. Use was made of the most complete kinetic data presently on chemical reactions in hot air. One can clearly see the nonmonotonic (with the formation of a density maximum $n_{\text{NO}} \approx 10^{17}$ cm^{-3} at the points in time $t \sim \tau_{\max} \approx 10^{-7}-10^{-3}$ s) approach of the $n_{\text{NO}}(T, t)$ dependence to the thermodynamically equilibrium values for moderate temperatures ($T \geqslant 4000$ K). This behavior of the time dependence of n_{NO} permits obtaining superequilibrium NO densities in the rapid expansion (with a characteristic time $\tau_{\text{exp}} \sim \tau_{\max}$) of the heated air.

estimating the temperature at which the volume content of NO stops to change — the nitrogen oxide quenching (or 'freezing') temperature T_q. Knowing T_q and using the thermodynamically equilibrium content of nitrogen oxide in heated air (for instance, as borrowed from Ref. [57]), it is easy to estimate the amount of (quenched) NO persisting in a lightning channel.

Figure 10 shows the thermodynamically equilibrium air composition at different temperatures and pressures. The temperature dependences of the volume content in the hot air are given for molecular nitrogen (N_2), molecular oxygen (O_2), nitrogen oxide (NO), atomic nitrogen (N), and oxygen (O). We note that the highest content, $n_{\text{NO}} \approx 0.1$, is observed for hot air temperatures $T \approx 3000-4500$ K.

The NO formation kinetics must be known in order to determine $\tau_{\text{NO}}(T)$; such data, in particular, are given in Fig. 11, which shows how the characteristic settling time $\tau_{\text{NO}}(T)$ of thermodynamically equilibrium nitrogen oxide density varies in relation to the hot air temperature T. One can see that $\tau_{\text{NO}}(T)$ varies over several orders of magnitude in

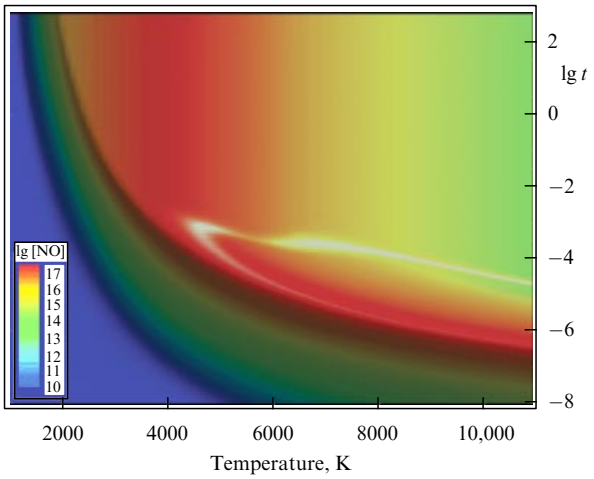

Figure 12. (Color online.) Kinetics of NO production in hot dry air. Shown is the two-dimensional dependence of the density $n_{NO}(t, T)$ on the time and the temperature. The color is determined by the $n_{NO}(t, T)$ value, which increases from blue to red, as indicated in the inset. One can clearly see the transition from the nonmonotonic increase of n_{NO} with time to the monotonic one, which is observed for $T \approx 4000$ K, and the variation of the settling time of the thermodynamically equilibrium nitrogen oxide density $\tau_{NO}(T)$ with increasing temperature. The air density $\rho_a = 10^{-4}$ g cm^{-3}.

a narrow temperature range ($T \approx 2000-3000$ K), which results in the effect of NO freezing on cooling of the hot air. The inset in Fig. 11 shows the NO production kinetics at different temperatures (we note that the NO kinetics as a function of time and temperature are more clearly shown in Fig. 12). One can see the nonmonotonic (with the formation of a density peak $n_{NO} \approx 10^{17}$ cm^{-3} for a time period $t \sim \tau_{max} \approx 10^{-7}-10^{-3}$ s) approach of the $n_{NO}(T, t)$ dependence to the thermodynamically equilibrium values at moderate temperatures ($T \geqslant 4000$ K). We emphasize that this behavior of the time dependence of n_{NO} provides the possibility of obtaining superequilibrium NO densities in the rapid expansion (with a characteristic time $\tau_{exp} \sim \tau_{max}$) of heated air. This conclusion will probably lead to a reevaluation (towards higher values) of the global amount of nitrogen oxide produced in lightning discharges. Figure 13 shows the kinetics of several compounds of importance in atmospheric chemistry for the temperature range characteristic for lightning discharges at their cooling stage. Apart from the quasiequilibrium contents of these compounds, these dependences also show the characteristic transition times to thermodynamic equilibrium.

It is possible to analytically estimate $\tau_{NO}(T)$ by using the key reactions which determine the losses of NO in hot air:

$$\begin{aligned} &NO + N \rightarrow N_2 + O\,, \\ &NO + O \rightarrow N + O_2\,, \\ &NO + O_2 \rightarrow NO_2 + O\,, \end{aligned} \qquad (6)$$

with the respective rate coefficients $k_1 \approx 10^{-12}\sqrt{T}$ cm^3 s^{-1}, $k_2 \approx 2.5 \times 10^{-15}\, T \exp(-19500\ \mathrm{K}/T)$ cm^3 s^{-1}, and $k_3 \approx 3 \times 10^{-12} \exp(-23400\ \mathrm{K}/T)$ cm^3 s^{-1} of the three reactions. Consequently, the characteristic lifetime τ_{NO} of an NO molecule in heated air is defined as follows: $\tau_{NO} \approx (k_1[N] + k_2[O] + k_3[O_2])^{-1}$, where [N], [O], and [$O_2$] are the densities of atomic nitrogen and oxygen and of molecular oxygen. The data of thermodynamic calculations given in Fig. 10 suggest that the contributions from k_1[N] and k_2[O]

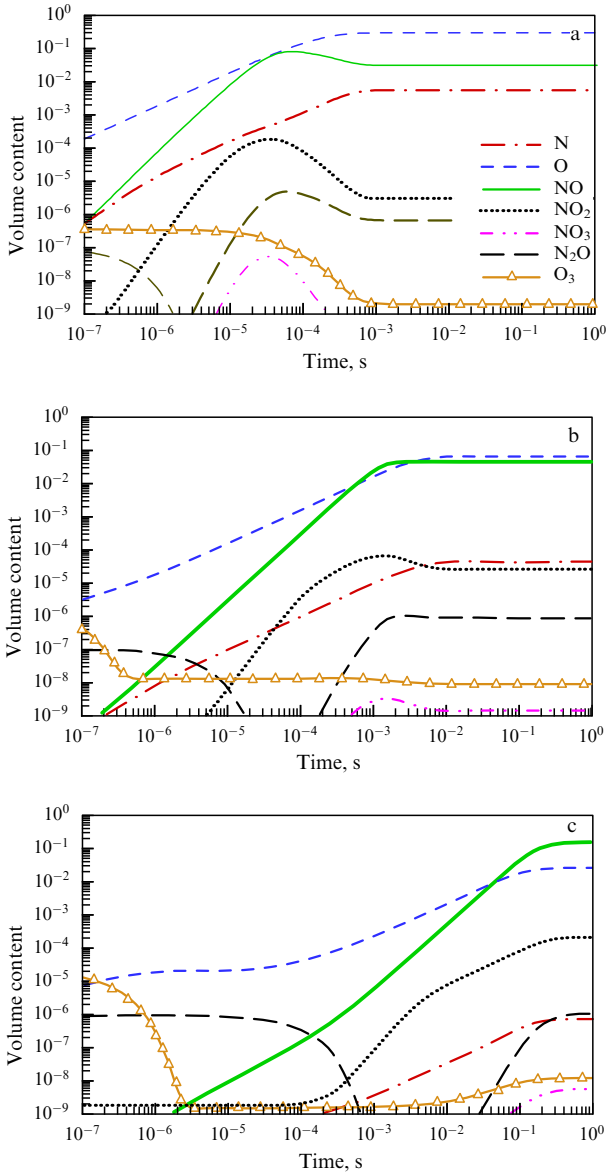

Figure 13. Kinetics of minor constituents (compounds), important for atmospheric photochemistry, in heated dry air at different temperatures: 5000 K (a), 3500 K (b), and 2500 K (c). Presented are the time dependences of the volume densities of atomic nitrogen (N) and oxygen, ozone (O_3), and the nitrogen compounds NO, NO_2, NO_3, and N_2O. The air density $\rho_a = 10^{-4}$ g cm^{-3}.

may be neglected owing to their smallness in comparison with k_3[O_2] for temperatures $T_h \leqslant 2500$ K in a wide range of hot air pressures. In this case, it is possible to obtain a simple estimate for τ_{NO}:

$$\tau_{NO} \sim (k_3[O_2])^{-1} \approx 10^{-7} \exp\left(\frac{23{,}400\ \mathrm{K}}{T}\right) \frac{\rho_0}{\rho_a}\,.$$

It is seen that a lowering of the hot air temperature results in a sharp lengthening of the characteristic settling time of the thermodynamic equilibrium[2] for NO; this is also clearly seen

[2] It is noteworthy that the last reaction in (6) was disregarded in pioneering work [48], and thereby the thermodynamic equilibrium settling time for NO turned out to be greatly overestimated and, accordingly, the amount of NO frozen in the expansion of the hot cloud was also greatly overestimated.

in Fig. 11, which corresponds to a substantially more comprehensive scheme of chemical reactions. This kinetic scheme included the nine most important dry air compounds: N_2, O_2, N, O, NO, NO_2, N_2O, NO_3, O_3, and 40 reactions between them from Ref. [56]. This scheme was verified by attaining equality of the quasistationary (equilibrated) densities of the above compounds and their equilibrium values in the temperature range (2000–6000 K) under consideration.

Therefore, the hot air oxidation mechanism proposed by Ya B Zeldovich provides an excellent qualitative explanation for the production of nitrogen oxide and its freezing: in the expansion of the hot air, the characteristic time $\tau_{NO}(T)$ sharply increases with a decrease in temperature. For $\tau_{NO}(T_q) \approx \tau_c$, NO is observed to freeze: the NO fraction in the hot gas is hardly changed and approximately corresponds to the thermodynamically equilibrium NO fraction at the instant of freezing (and at the 'freezing' temperature T_q).

However, a quantitative description of NO freezing requires not only the characteristic cooling time τ_c determined by the gas-dynamic expansion of the hot gas and its subsequent mixing (and cooling) with the surrounding cool air, but also the spatio-temporal behavior of the density ρ and temperature T of the expanding gas. Hence, it is possible to rather easily calculate the amount of resultant nitrogen oxides by using a detailed kinetic reaction scheme. In the case of a linear lightning discharge under consideration, an additional advantage is the discharge symmetry: this problem may be treated within a cylindrical symmetry approximation.

During this discharge, the gas in the trunk of a lightning channel is heated to temperatures $T \approx (2.5-3) \times 10^4$ K in a time on the order of several microseconds [58, 59]. At these temperatures, molecular nitrogen and oxygen are completely dissociated, and the degree of ionization in the gas is close to unity. When describing the expansion of this hot gas, without loss in generality we may take the following initial parameters of the lightning channel: the temperature of the hot air $T_h \approx 3 \times 10^4$ K, its density ρ_h is equal to the ambient air density ρ_a, $\rho_h \approx 10^{-4}$ g cm^{-3}, the ambient air pressure $p_a \sim 0.1$ bar. The initial radius of the lightning channel $r_0 \approx 3$ cm, its length $L \approx 5$ km. These parameters correspond to a discharge energy $E_0 \sim 10^{15}$ erg, which is typical for a single return stroke (see, for instance, Ref. [58]).

Under the above conditions, the initial pressure in the lightning channel $p_h \approx 40$ bar (the complete dissociation of the air molecules and the single ionization of N and O atoms are taken into account). The ratio $p_h/p_a \sim 10^3 \gg (\gamma+1)/(\gamma-1) \sim 10$, where γ is the adiabatic exponent ($\gamma \approx 1.2$ for the parameters under consideration), and a strong shock wave is therefore produced in the expansion of the hot air of the lightning channel. The initial shock velocity D_0 can be estimated from the relation $D_0 \simeq \sqrt{2p_h/(\gamma+1)\rho_a}$. Initially, $\gamma \approx 1.2$ and $D \approx 6 \times 10^5$ cm s^{-1}.

We emphasize that the characteristic velocity v_{rs} of return stroke propagation is much higher: $v_{rs} \sim 10^9 - 10^{10}$ cm s^{-1} [59–61]. That is why the approximation of a strong cylindrical explosion is the most adequate one for describing the expansion of a lightning channel. In this case, the shock velocity D lowers with distance r from the line of explosion: $D \approx D_0(r_0/r)$. The temperature T_f behind the SW front may be estimated from relation [42], $T_f \propto p_f/\rho_f \approx p_f/\rho_a(\gamma-1)/(\gamma+1) \propto D^2 \propto r^{-2}$. In the lightning channel, the time of gas cooling is estimated as $\tau_c \sim r_h/c_s \sim 10^{-3}$ s, where r_h is the lightning channel radius ($r \approx 1$ m), and c_s is the sonic speed in the heated air. The NO freezing temperature in this case, as is easily verified in Fig. 11, is about 2500 K. Then, the amount of nitrogen oxide NO frozen in the course of the lightning channel expansion will be about 1% of the mass of air heated to the temperature exceeding the freezing temperature T_q. This amount may be shown to depend only slightly on the magnitude of T_q, and the amount of resultant nitrogen oxide per unit discharge energy depends only slightly on the ambient air pressure p_a.

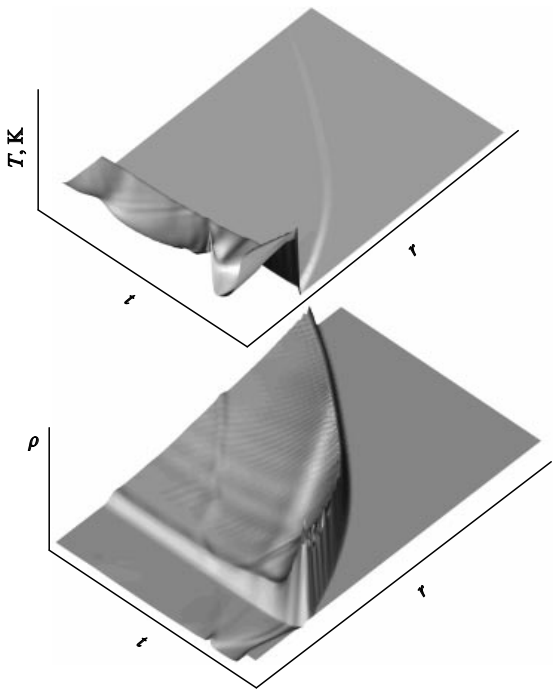

Figure 14. Spatio-temporal evolution of a linear lightning discharge. Shown in the drawing are the qualitative dependences of the temperature T (a) and density ρ (b) on the time and mass Lagrangian coordinate r.The ambient air density $\rho_a = 10^{-4}$ g cm^{-3}. The shock wave formation and the production of a hot lightning channel with a density lower than ρ_a are clearly seen.

However, the amount of nitrogen oxides produced in the discharge may be determined with a substantially higher accuracy by way of numerical simulation of the lightning channel expansion involving the real equation of state of the hot air [57]. Some results of such simulations are given in Fig. 14, which shows the lightning channel evolution: the dependences of the temperature T and density ρ on the time and Lagrangian mass coordinate r. Clearly seen are the shock wave formation and the production of a low-density warm lightning channel late in the expansion. Here, the system of gas-dynamic equations was solved using a modified two-dimensional hydrodynamic code tested in the solution to several problems on a high-velocity liner–target interaction (which arise, for instance, in the description of the deceleration of a comet/asteroid in planetary atmospheres [62–66].

These calculations suggest that the amount frozen NO in the trunk of a lightning channel amounts to about 2–3% (which is close to the estimates given above) of the air initially heated in the discharge. Hence, it is easy to determine the energy expended to produce one NO molecule, $P(NO)$ — it is estimated at 70–100 eV per molecule. It is instructive to compare this figure with the efficiency of NO production in a plasmatron [67] (in this case [$P(NO) \approx 10$ eV per molecule] and chemical explosions in the air [42] [$P(NO) \approx 150-200$ eV

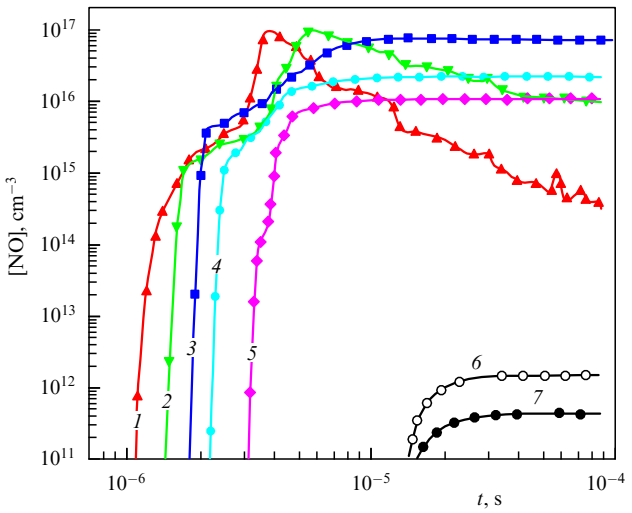

Figure 15. (Color online.) Production of nitrogen oxide (NO) behind the shock front in the expansion of a linear lightning discharge. The time dependences of NO density are plotted for several mass Lagrangian coordinates at different distances from the symmetry axis. The variation of curve color from red to lilac corresponds to the increase in distance from the central discharge region. Black curves correspond to boundary discharge regions, where the production of NO is less efficient. The NO freezing is evident in the majority of the dependences presented. The ambient air density is 10^{-4} g cm^{-3}.

per molecule]. Some estimates of $P(\mathrm{NO})$ are given in Ref. [68], according to which $P(\mathrm{NO})$ varies between 30 and 200 eV per molecule. The relatively high energy price for NO production in chemical explosions is due to the greater spatial scale of the process and, accordingly, to the longer characteristic time of hot gas cooling: under these conditions, nitrogen oxide is converted to N_2 and O_2 with a higher efficiency, in accordance with the data of Fig. 10.

Some NO formation data obtained with the inclusion of the gas-dynamic processes of shock wave generation and lightning channel expansion are presented in Fig. 15, which shows the time dependence of the NO density for several Lagrangian coordinates. The 'freezing' of nitrogen oxide in the expanding gas is evident. When the initial temperature in the trunk of the lightning channel is moderate, $T \approx 2 \times 10^4$ K, nitrogen oxide is produced primarily in the discharge region, in the hot trunk, and the contribution from the SW is insignificant. In this case, the magnitude of $P(\mathrm{NO})$ depends only slightly on the ambient air pressure and is about the same [$P(\mathrm{NO}) \approx 100$ eV per molecule] at altitudes of the troposphere and lower stratosphere. For high-power discharges and high initial temperatures ($T \approx 3 \times 10^4$ K), the situation is the reverse: the shock wave plays the crucial role in the production of nitrogen oxide.

So, in a lightning discharge a large amount of NO forms, the level of NO in the trunk of the lightning channel being much higher than in the unperturbed ambient air. For instance, the initial density of frozen nitrogen oxide in the warm ($T \leqslant 2500$ K) lightning channel $n_{\mathrm{NO}}^{\mathrm{lig}} \sim 10^{15} - 10^{17}$ cm^{-3} for a typical return discharge at altitudes where $p_a = 0.1$ bar (which corresponds to an altitude of about 15 km), while the 'quasiequilibrium' (determined by the level of solar activity and photochemical processes) NO density in the ambient air at stratospheric altitudes, $n_{\mathrm{NO}}^{\mathrm{n}}$, does not usually exceed 10^9 cm^{-3}, i.e., is much lower. Turbulent mixing and diffusion lower the level of NO in the lightning channel trunk, forming in it an air column with a strongly nonequilibrium NO content. The spatio-temporal parameters of this column may be estimated from the solution of the diffusion equation neglecting photochemical processes; this solution is of the form

$$n_{\mathrm{NO}}(r, t) \propto \frac{\exp\left(-r^2/K_{\mathrm{D}}t\right)}{t},$$

where K_{D} is the turbulent diffusion coefficient; in the stratosphere and upper troposphere, it may be estimated from the relation $K_{\mathrm{D}} \approx 8t^{1.6}$ cm^2 s^{-1} [69]. It is then easy to estimate the radial size r_{d} of the column with the nonequilibrium NO content: $r_{\mathrm{d}} \sim \left(n_{\mathrm{NO}}^{\mathrm{lig}}/n_{\mathrm{NO}}^{\mathrm{n}}\right)^{1/2} \approx 100$ m. The characteristic lifetime τ_{d} of this column relative to mixing and diffusion spreading may be estimated from the relation $r_{\mathrm{d}} \simeq \sqrt{K_{\mathrm{D}}\tau_{\mathrm{d}}} \simeq 3\tau_{\mathrm{d}}^{1.3}$; hence, $\tau_{\mathrm{d}} \sim 300$ s.

The excess of nitrogen oxide in this air column produces a local ozone depression at stratospheric altitudes, which is caused by the catalytic reaction $\mathrm{NO} + \mathrm{O_3} \rightarrow \mathrm{NO_2} + \mathrm{O_2}$ with the rate coefficient

$$k_4 \approx 4 \times 10^{-12} \exp\left(-\frac{1560\ \mathrm{K}}{T}\right)\ \mathrm{cm^3\ s^{-1}}.$$

We note that the lifetime $\tau_{\mathrm{NO_2}}$ of nitrogen dioxide NO_2, which is produced by this reaction, relative to photolysis ($\mathrm{NO_2} + h\nu \rightarrow \mathrm{NO} + \mathrm{O}$), in which the resultant oxygen atom goes primarily to recover ozone ($\mathrm{O_2} + \mathrm{O} + \mathrm{M} \rightarrow \mathrm{O_3} + \mathrm{M}$), amounts to about 100 s, i.e., is on the order of τ_{d}. Consequently, the radial size r_{oz} of the column almost completely depleted in ozone may be determined from the relation $[k_3 n_{\mathrm{NO}}(r_{\mathrm{oz}}, t)]^{-1} \approx \tau_{\mathrm{NO_2}}$. This yields $r_{\mathrm{oz}} \approx 100$ m for the lightning stroke parameters under consideration.

Therefore, a lightning discharge in the lower stratosphere produces a local (on a scale of about 100 m) transient (with a characteristic lifetime on the order of 100 s) ozone depression. In this case, the discharge in the lower stratosphere ($h \geqslant 15$ km) annihilates $\sim \pi r_{\mathrm{oz}}^2 \delta_{\mathrm{oz}} L \rho_{\mathrm{s}} \approx 3$ kg of ozone, where δ_{oz} is the ozone mass fraction at the altitudes under consideration. Here, we do not estimate the additional production of nitrogen oxide in the air breakdown due to runaway electrons [59, 70, 71]. Such breakdowns are frequently observed in lightning discharges, but the efficiency of NO production caused by the action of this mechanism in the troposphere and stratosphere is, as is easily shown, insignificant in comparison with the efficiency of NO production due to the Zeldovich mechanism.

The total contribution ($\sim 10^9$ discharges per year) from lightning discharges to the production of nitrogen oxides may range up to $\sim 20\%$ of their total generated amount. However, the fraction of stratospheric discharges, which can affect the ozone level, is relatively small, and therefore the contribution of NO to ozone depletion is insignificant. It is noteworthy that the production of nitrogen oxide in a hot meteorite trail and the subsequent ozone depletion [65] were quite recently confirmed by satellite observations (Meteosat) of the Chelyabinsk meteorite in February of 2013 [72].

5. Conclusions

Presented in our review is the development of Ya B Zeldovich's ideas, some of which he proposed back in the mid-1930s as a young man in his twenties. Virtually all of his work

discussed above, beginning with the description of combustion waves and detonation theory and ending with the revelation of the nitrogen oxidation mechanism, evolved into major lines and fields of basic and applied science, not infrequently determining their development. And this is merely a small part of his tremendous contribution to basic science. To recognize what a unique personality Ya B Zeldovich was, to this must be added his popularization activity.

References

1. Zel'dovich Ya B, Frank-Kamenetskii D A *Dokl. Akad. Nauk SSSR* **19** 693 (1938)
2. Zel'dovich Ya B, Frank-Kamenetskii D A *Zh. Fiz. Khim.* **12** (1) 100 (1938)
3. Zeldovich Y B *Theory of Flame Propagation* (Technical Memorandum 1282) (Washington: National Advisory Committee for Aeronautics, 1951); Translated from Russian: Zel'dovich Ya B *Zh. Fiz. Khim.* **22** (1) 27 (1948)
4. Zeldovich Ya B, Barenblatt G I *Combust. Flame* **3** (1) 61 (1959)
5. Zel'dovich Ya B *Kinet. Kataliz* **2** 305 (1961)
6. Zeldovich Ia B, Kompaneets A S *Theory of Detonation* (New York: Academic Press, 1960); Translated from Russian: *Teoriya Detonatsii* (Moscow: Gos. Izd. Tekhniko-Teoret. Lit., 1955)
7. Zeldovich Ya B *Combust. Flame* **39** 211 (1980)
8. Kolmogorov A N, Petrovskii I G, Piskunov N S *Byull. MGU. Mat. Mekh.* **1** (6) 1 (1937); Kolmogorov A N *Selected Works* Vol. 1 (Ed. V M Tikhomirov) (Dordrecht: Kluwer Acad. Publ., 1991) p. 242; Translated from Russian: *Izbrannye Trudy. Matematika i Mekhanika* (Exec. Ed. S M Nikol'skii) (Moscow: Nauka, 1985) p. 221
9. Zeldovich Ya B et al. *Astron. Acta* **15** 313 (1970)
10. Gel'fand B E et al. *Fiz. Goren. Vzryva* (4) 118 (1985)
11. He L *Combust. Flame* **104** 401 (1996)
12. Kapila A K et al. *Combust. Theory Model.* **6** 553 (2002)
13. Sharpe G J, Short M *J. Fluid Mech.* **476** 267 (2003)
14. Mechik K A et al. *Nonequilibrium Processes* Vol. 1 (Eds G D Roy, S M Frolov, A M Starik) (Moscow: Torus Press, 2005) p. 324
15. Liberman M A, Kiverin A D, Ivanov M F *Phys. Rev. E* **85** 056312 (2012)
16. Konnov A A *Khim. Fiz.* **23** (8) 5 (2004)
17. Kusharin A Y et al. *Combust. Sci. Technol.* **135** 85 (1998)
18. Ó Conaire M et al. *Int. J. Chem. Kinet.* **36** 603 (2004)
19. Warnatz J, Maas U, Dibble R W *Combustion*: *Physical and Chemical Fundamentals, Modeling and Simulation, Experiments, Pollutant Formation* (Berlin: Springer, 2006)
20. Ivanov M F et al. *Dokl. Phys.* **55** 480 (2010); *Dokl. Ross. Akad. Nauk* **434** 756 (2010)
21. Gu X J, Emerson D R, Bradley D *Combust. Flame* **133** 63 (2003)
22. Maas U, Warnatz J *Combust. Flame* **74** 53 (1988)
23. Kiverin A D et al. *Phys. Rev. E* **87** 033015 (2013)
24. Coward H F, Jones G W "Limits of flammability of gases and vapors", Bulletin 503 (Washington: U.S. Bureau of Mines, 1952); http://digicoll.manoa.hawaii.edu/techreports/PDF/USBM-503.pdf
25. "Mitigation of Hydrogen Hazards in Severe Accidents in Nuclear Power Plants", IAEA-TECDOC-1661 (Vienna: IAEA, 2011); http://www-pub.iaea.org/MTCD/publications/PDF/TE_1661_Web.pdf
26. Bach G G, Knystautas R, Lee J H *Symp.* (*Int.*) *Combust.* **12** 853 (1969)
27. Urtiew P A, Oppenheim A K *Proc. R. Soc. Lond. A* **295** 13 (1966)
28. Oran E S, Gamezo V N *Combust. Flame* **148** 4 (2007)
29. Ivanov M F, Kiverin A D, Liberman M A *Phys. Rev. E* **83** 056313 (2011)
30. Ivanov M F, Kiverin A D, Galburt V A *Combust. Sci. Technol.* **182** 1683 (2010)
31. Zel'dovich Ya B *Zh. Tekh. Fiz.* **17** (1) 3 (1947)
32. Gostintsev Yu A, Istratov A G, Fortov V E *Dokl. Phys. Chem.* **353** 83 (1997); *Dokl. Ross. Akad. Nauk* **353** 55 (1997)
33. Liberman M A et al. *Phys. Fluids* **16** 2476 (2004)
34. Shchelkin K I *Dokl. Akad. Nauk SSSR* **23** 636 (1939)
35. Shchelkin K I *Sov. Phys. Usp.* **8** 780 (1966); *Usp. Fiz. Nauk* **87** 273 (1965)
36. Ivanov M F, Kiverin A D, Liberman M *Int. J. Hydrogen Energy* **38** 16427 (2013)
37. Kuznetsov M et al. *Shock Waves* **14** 205 (2005)
38. Salamandra G D, Bazhenova T V, Naboko I M *Symp.* (*Int.*) *Combust.* **7** 851 (1959)
39. Wu M et al. *Proc. Combust. Inst.* **31** 2429 (2007)
40. Zeldovich Ya B *Acta Physicochim. USSR* **21** 577 (1946)
41. Zel'dovich Ya B, Sadovnikov P Ya, Frank-Kamenetskii D A *Okislenie Azota pri Gorenii* (Oxidation of Nitrogen in Combustion) (Moscow–Leningrad: Izd. AN SSSR, 1947)
42. Zel'dovich Ya B, Raizer Yu P *Physics of Shock Waves and High-Temperature Hydrodynamic Phenomena* (Mineola, N.Y.: Dover Publ., 2002); Translated from Russian: *Fizika Udarnykh Voln i Vysokotemperaturnykh Gidrodinamicheskikh Yavlenii* (Moscow: Nauka, 1966)
43. Zel'dovich Ya B "Okislenie azota pri gorenii" ("Oxidation of nitrogen in combustion"), Dissertation for Doctor of Physics and Mathematics (Leningrad: Institute of Chemical Physics, 1939)
44. von Liebig J *Ann. Chim. Phys.* **35** 329 (1827)
45. Goldsmith P et al. *Nature* **244** 545 (1973)
46. Noxon J F *Geophys. Rev. Lett.* **3** 463 (1976)
47. Chameides W L et al. *J. Atmos. Sci.* **34** 143 (1977)
48. Chameides W L *Nature* **277** 123 (1979)
49. Goldenbaum G C, Dickerson R R *J. Geophys. Res.* **98** (D10) 18333 (1993)
50. Crutzen P J *Quart. J. R. Meteorol. Soc.* **96** 320 (1970)
51. Rowland F S, Molina M J *Rev. Geophys. Space Phys.* **13** (1) 1 (1975)
52. Crutzen P J *Annu. Rev. Earth Planet. Sci.* **7** 443 (1979)
53. Solomon S *Rev. Geophys.* **37** 275 (1999)
54. Schumann U, Huntrieser H *Atmos. Chem. Phys.* **7** 3823 (2007)
55. Christian H J et al. *J. Geophys. Res.* **108** (D1) 4005 (2003)
56. DeMore W B et al. *Chemical Kinetics and Photochemical Data for Use in Stratospheric Modeling Evaluation* (Pasadena, Calif.: Jet Propulsion Lab., 2011) p. 17
57. Kuznetsov N M *Termodinamicheskie Funktsii i Udarnye Adiabaty Vozdukha pri Vysokikh Temperaturakh* (Thermodynamic Functions and Shock Adiabats of the Air at High Temperatures) (Moscow: Mashinostroenie, 1965)
58. Ogawa T, in *Handbook of Atmospheric Electrodynamics* Vol. 1 (Ed. H Volland) (Boca Raton, Fl.: CRC Press, 1995) p. 93
59. Dwyer J R, Uman M A *Phys. Rep.* **534** 147 (2014)
60. Bazelyan E M, Raizer Yu P *Phys. Usp.* **43** 701 (2000); *Usp. Fiz. Nauk* **170** 753 (2000)
61. Rakov V A, Uman M A *Lightning*: *Physics and Effects* (Cambridge: Cambridge Univ. Press, 2003)
62. Stone J M, Norman M L *Astrophys. J. Suppl.* **80** 753 (1992)
63. Klumov B A et al. *Phys. Usp.* **37** 577 (1994); *Usp. Fiz. Nauk* **164** 617 (1994)
64. Fortov V E et al. *Phys. Usp.* **39** 363 (1996); *Usp. Fiz. Nauk* **166** 391 (1996)
65. Klumov B A *JETP Lett.* **70** 363 (1999); *Pis'ma Zh. Eksp. Teor. Fiz.* **70** 360 (1999)
66. Klumov B A et al. *Phys. Usp.* **48** 733 (2005); *Usp. Fiz. Nauk* **175** 767 (2005)
67. Rusanov V D, Fridman A A *Fizika Khimicheski Aktivnoi Plazmy* (The Physics of Chemically Active Plasma) (Moscow: Nauka, 1984)
68. Lawrence M G et al., in *Handbook of Atmospheric Electrodynamics* Vol. 1 (Ed. H Volland) (Boca Raton, Fl.: CRC Press, 1995) p. 189
69. *The Natural Stratosphere of 1974* (CIAP Monograph) (Springfield, VA: US Dept. Commerce, 1975)
70. Gurevich A V et al. *Phys. Usp.* **52** 735 (2009); *Usp. Fiz. Nauk* **179** 779 (2009)
71. Gurevich A V, Zybin K P *Phys. Usp.* **44** 1119 (2001); *Usp. Fiz. Nauk* **171** 1177 (2001)
72. Borovička J, Private communication (2013)